

VIBRATIONS IN PHYSICAL SYSTEMS

Volume 28

Editors

Czesław CEMPEL

Tomasz STREK

Maciej TABASZEWSKI

Poznan 2017



VIBRATIONS IN PHYSICAL SYSTEMS

Vol. 28, 2017

ISSN 0860-6897

EDITORIAL OFFICE

Poznan University of Technology

Institute of Applied Mechanics

ul. Jana Pawla II 24, 61-139 Poznan, Poland

tel. +48 61 665 23 01, fax: +48 61 665 23 07

e-mail: office_am@put.poznan.pl

www.vibsys.put.poznan.pl

EDITORIAL BOARD

HONORARY EDITOR

Czesław CEMPEL

EDITORS

Tomasz STREK, Maciej TABASZEWSKI

TECHNICAL EDITORS

Paweł FRITZKOWSKI, Hubert JOPEK (web page), Tomasz HERMANN (typeset)

EDITORIAL BOARD MEMBERS

Vladimir I. ALSHITS, Jan AWREJCEWICZ, Wojciech BATKO, Romuald BĘDZIŃSKI,
Roman BOGACZ, Tadeusz BURCZYŃSKI, Czesław CEMPEL, Enzo CIANCIO,
Evgen CZAPLA, Zbigniew DĄBROWSKI, Marian W. DOBRY, Antoni GAJEWSKI,
Joseph GRIMA, Jan HOLNICKI-SZULC, Erik V. JANSSON, Jarosław JĘDRYSIAK,
Stefan JONIAK, David JOU, Jerzy KALETA, Jan KOŁODZIEJ, Tomasz ŁODYGOWSKI,
Krzysztof MAGNUCKI, Krzysztof MARCHELEK, Bogdan MARUSZEWSKI,
Stanisław MATYSIAK, Wolfgang MUSCHIK, Józef NIZIOL, Andrzej RADOWICZ,
Stanisław RADKOWSKI, Liliana RESTUCCIA, Hamid M. SEDIGHI, Roman STAROSTA,
Tomasz STREK, Tomasz SZOLC, Maciej TABASZEWSKI, Franciszek TOMASZEWSKI,
Andrzej TYLIKOWSKI, Tadeusz UHL, Jerzy WARMIŃSKI,
Józef WOJNAROWSKI, Alexandr YAVLENSKY

REVIEWERS OF PAPERS

Wojciech BATKO, Czesław CEMPEL, Paweł FRITZKOWSKI, Piotr KĘDZIA,
Jarosław JĘDRYSIAK, Hubert JOPEK, Mirosław NADER, Hamid M. SEDIGHI,
Roman STAROSTA, Grzegorz SZYMAŃSKI, Maciej TABASZEWSKI

Cover design: Piotr GOŁĘBNIAK

PRINTED

Agencja Reklamowa COMPRINT

ul. H. Rzepeckiej 26 A, 60-465 Poznan, Poland

Tel. +48 602 26 64 26, e-mail: comprint@data.pl, www.comprint.com.pl

© Copyright by Poznan University of Technology, Poznan, Poland 2017

Edition based on ready-to-publish materials submitted by authors.

No part of this work may be reproduced, stored in a retrieval system, or transmitted in any form or by any means, electronic, mechanical, photocopying, microfilming, recording or otherwise, without written permission from the copyright owner.

The volume was published in the cooperation of the Institute of Applied Mechanics at Poznan University of Technology and Polish Society of Theoretical and Applied Mechanics.

Vibrations in Physical Systems is indexed in SCOPUS, Baz Tech and POL-INDEX.

This journal is indexed in the list of Ministry of Science and Higher Education (5 points).

CONTENTS

PAPERS

1. **Tomasz HERMANN, Marian W. DOBRY..... 2017001**
ASSESSMENT OF THE EFFECTIVENESS OF ANTI-VIBRATION
GLOVES. A COMPARISON OF THE CONVENTIONAL
AND ENERGY METHOD. INTRODUCTION – PART ONE
2. **Tomasz HERMANN, Marian W. DOBRY..... 2017002**
ASSESSMENT OF THE EFFECTIVENESS OF ANTI-VIBRATION
GLOVES. A COMPARISON OF THE CONVENTIONAL
AND ENERGY METHOD. ANALYSIS AND INTERPRETATION OF
RESULTS – PART TWO
3. **Eligiusz IDCZAK, Tomasz STRĘK..... 2017003**
DYNAMIC ANALYSIS OF OPTIMIZED TWO-PHASE AUXETIC
STRUCTURE
4. **Bartosz JAKUBEK, Roman BARCZEWSKI,
Michał JAKUBOWICZ 2017004**
THE INFLUENCE OF THE LUBRICATION ON
THE VIBROACOUSTIC SIGNAL GENERATED BY ROLLING
BEARINGS
5. **Maciej TABASZEWSKI, Małgorzata WOJSZNIŚ 2017005**
EVALUATION OF A SIMPLE METHOD OF IDENTIFICATION OF
DYNAMIC PARAMETERS OF A SINGLE-DEGREE-OF-FREEDOM
SYSTEM
6. **Mateusz WRÓBEL, Roman BARCZEWSKI..... 2017006**
A SMALL-SIZE STAND FOR VIBROACOUSTIC
AND DURABILITY TESTING OF ROLLING BEARINGS
7. **Korabathina RAJESH, Koppanati Meera SAHEB..... 2017007**
LARGE AMPLITUDE FREE VIBRATION ANALYSIS OF TAPERED
TIMOSHENKO HINGED-HINGED BEAM USING COUPLED
DISPLACEMENT FIELD METHOD

- 8. Vladimir ZASELSKIY, Dmitry POPOLOV,
Igor ZASELSKIY 2017008**
THEORETICAL DETERMINATION OF WEAR
AND LIFETIME OF THE SCREEN SOWING SURFACE
- 9. Wojciech RUKAT, Bartosz JAKUBEK 2017009**
THE INFLUENCE OF THE CUTTING TOOTH DESIGN
AND WEAR OF A SAW CHAIN ON THE VIBRATION LEVEL OF
A CHAINSAW

Assessment of the Effectiveness of Anti-Vibration Gloves. A Comparison of the Conventional and Energy Method. Introduction – Part One

Tomasz HERMANN

*Poznan University of Technology, Institute of Applied Mechanics
Jana Pawla II 24, Poznan, tomasz.hermann@put.poznan.pl*

Marian Witalis DOBRY

*Poznan University of Technology, Institute of Applied Mechanics
Jana Pawla II 24, Poznan, marian.dobry@put.poznan.pl*

Abstract

The article is an introduction to the assessment of the effectiveness of anti-vibration gloves. The assessment was conducted for a specific glove. The impact of the glove was taken into account in a model of the biodynamic system consisting of the human operator, the anti-vibration glove and the hand-held power tool. The synthetic model was created by integrating the physical model of the human body and the glove model specified in the International Standard ISO 10068:2012 with a model of an electric angle grinder. The first part of the study describes an alternative model of the glove, developed on the basis of experimental data. The article also presents a description of dynamic and energy models for analyzing dynamic structures of the biomechanical system. Results obtained at this stage are used to analyse and interpret the observed phenomena and to compare methods of assessing the effectiveness of anti-vibration gloves, which are discussed in detail in the second part.

Key words: biomechanical system, local vibrations, energy method of assessment

1. Introduction

Studies involving discrete models of the human body were already conducted in the 1970s. Major contributions in this field were made by Griffin [6], Meltzer [7] and Reynolds [8]. Nowadays this problem is being studied by other researchers [3–5].

It is worth noting that most of those analyses have focused mainly on the response generated by the model, which should always be similar to the result produced by the real system. While this is no doubt a major criterion in modelling, it is also necessary to consider the internal structure of the model, which will be fully compatible with the real system not only when it generate a specific response but also when its internal structure is sufficiently well defined.

The present article is an introduction to a comparative assessment of the impact of vibrations on the human operator using an anti-vibration glove. Two methods of assessment were applied: the conventional and the energy method. For this purpose, the physical model of the human body and the model of the glove specified in the ISO 10068:2012 standard were used. In addition, the assessment was based on experimental data for a specific anti-vibration glove, which satisfied safety requirements for this kind of personal protective equipment according to industrial standards [10, 11].

2. Results of laboratory measurements

The necessary laboratory measurements were conducted in the Laboratory of Dynamics and Ergonomics of the Human-Technical Object-Environment Metasystem at Poznan University of Technology using the Brüel & Kjær integrating vibration meter, type 2513. The meter was set to read RMS values of vibration accelerations, which were averaged during each reading with a 1 second time constant. The linear weighting was selected, which means that no filters were used and the measurement frequency range was between 10 and 10,000 Hz. The experimental setting was designed to represent the case of an operator using an angle grinder with a 125 mm disc and a rotation speed of 11,000 rpm.

Accelerations of vibrations in the human body separately in three directions, i.e. along the x , y and z axis, were measured. However, in the article we only present results of vibrations along the dominant direction, i.e. the z axis. It is worth noting that it is often the most important direction analysed in tests of various tools. The purpose of measurements was to obtain input data along the specified direction of movement for subsequent numerical simulations. The test was designed to recreate the following three conditions:

- a) when the tool is used without the glove – RMS values of vibration accelerations at the handle were measured, which are equivalent to RMS values of vibration accelerations experienced by the operator, i.e. at the contact surface between the palm and the handle,
- b) when the operator uses an anti-vibration glove – RMS values of vibration accelerations at the handle were measured, which have changed as a result of being gripped through the anti-vibration layer of the glove,
- c) when the operator uses an anti-vibration glove – RMS values of vibration accelerations at the contact surface between the operator's hand and the anti-vibration layer of the glove were measured.

Measurements for each condition were expressed as 2 numbers identifying particulars measurement series: the mean (the measure of central tendency) and standard deviation (the measure of dispersion). The precision of measurements burdened with random errors was determined using confidence intervals with Student's t -distribution. The confidence interval was set at 95% ($\alpha = 0.05$), with 9 degrees of freedom ($k = 9$, given 10 measurements for each condition). The critical value of the test statistic $t_{(\alpha;k)}$ for such criteria was obtained from statistical tables. Table 1 shows results for the three conditions.

Table 1. (RMS) values of vibration accelerations – laboratory measurements

Measurement condition	Value	Unit
at the handle (without the glove)	101.00 ± 2.82	m/s ²
at the handle (with the glove)	117.00 ± 6.79	
at the palm of the hand (with the glove)	26.55 ± 0.83	

It should be noted that the classic approach focusing on the vibration amplitude revealed a negative effect of the anti-vibration glove on RMS values of vibration accelerations on the handle. It turns out that the fact of holding the grinder through the

anti-vibration layer of the glove actually increases the amplitude of vibrations measured at the handle. Moreover, RMS values of vibrations at the handle without the glove are more consistent, i.e. less dispersed. This is confirmed by values of standard deviations shown in Table 1.

In addition, vibration acceleration signals generated by the grinder along the z axis were recorded using an oscilloscope. The experimental data to model signals of vibration accelerations for simulation purposes was used. The progressive mechanical wear of the disc, which was mainly due to its quality, caused a static imbalance. The grinding disc wore out unevenly, producing more complex patterns of oscilloscope signals. The basic section of acceleration signals consisted of six sines of varying amplitude and frequency. Figure 1 shows the signal of vibration accelerations used for purposes of simulation, which was modelled on the basis of signals recorded by the oscilloscope. Consistency of the modelled signal with the experimental data was confirmed by equal RMS values.

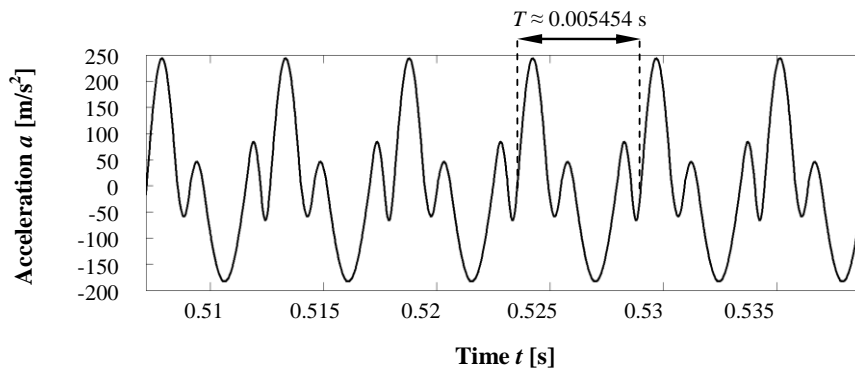


Figure 1. The signal curve of vibration accelerations at the handle modelled on the basis of recorded data, with the basic section indicated

The next stage of the study involved developing a model of the H – G – T system, consisting of the human operator (H), the anti-vibration glove (G) and the hand-held power tool (T). Figure 2 shows the combined biomechanical system, which consists of the physical model of the human body and the dynamic structure of the glove model presented in the ISO 10068:2012 standard [9]. These discrete models contain points of reduction, which are interconnected by damping and elastic elements. Values of the dynamic parameters for the model of the human body, i.e. m_i , k_i and c_i were taken from the ISO 10068:2012 standard [9].

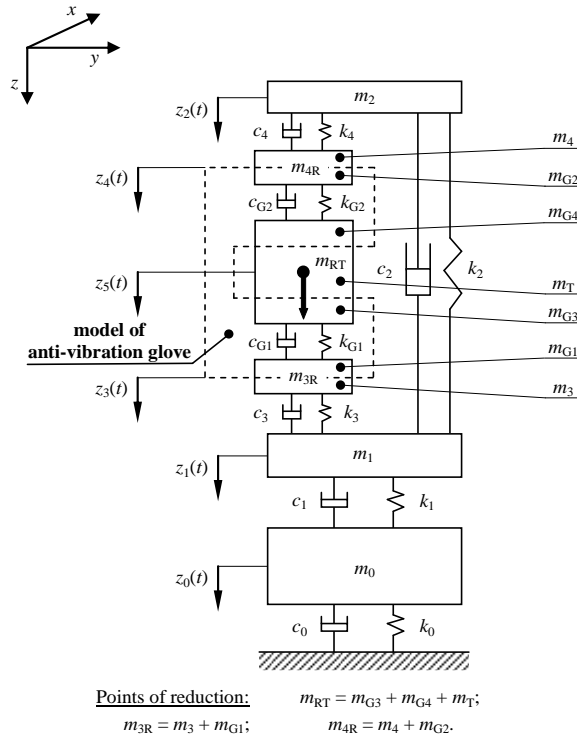


Figure 2. Physical model of the biodynamic H – G – T system created by combing the physical model of the human body and the glove model described in ISO 10068:2012 [9] with the tool model

Original values provided for the glove model were adapted to match the results of measurements obtained for the anti-vibration glove tested in the laboratory. The dynamic parameters for the glove, i.e. m_{Gi} , k_{Gi} and c_{Gi} are presented in Table 2.

Table 2. Values of dynamic parameters for the anti-vibration glove along the z axis

Parameter	Value	Unit
m_{G1}	0.0540	kg
m_{G2}	0.0140	
m_{G3}	0.0018	
m_{G4}	0.0013	
k_{G1}	10.60	N/m
k_{G2}	19.64	
c_{G1}	36.5	Ns/m
c_{G2}	36.0	

The third element of the H – G – T model – the model of the percussive tool – was represented by one concentrated mass m_T . Data for analysis came from measurements involving an angle grinder operated at the maximum speed of 11,000 rpm, i.e. at an operational frequency of 183.(3) Hz, with period $T \approx 0.005454$ – Fig. 1.

3. Theoretical results

The first step in the theoretical part was to derive mathematical models of the dynamic structures using Lagrange equations of the second kind given by:

$$\frac{d}{dt} \left(\frac{\partial E}{\partial \dot{q}_j} \right) - \frac{\partial E}{\partial q_j} = Q_j + Q_{jP} + Q_{jR} \quad j = 1, 2, \dots, s \quad (1)$$

where: E – kinetic energy of the system, q_j – generalized coordinates, \dot{q}_j – generalized velocities, Q_j – external active forces, Q_{jP} – potential forces, Q_{jR} – dissipative forces, s – number of degrees of freedom.

The mathematical model of the H – G – T system (Fig. 2) contains the following 6 generalized coordinates:

- $j = 1, \quad q_0 = z_0(t)$ – displacement of mass m_0 ,
- $j = 2, \quad q_1 = z_1(t)$ – displacement of mass m_1 ,
- $j = 3, \quad q_2 = z_2(t)$ – displacement of mass m_2 ,
- $j = 4, \quad q_3 = z_3(t)$ – displacement of masses m_3 and m_{G1} ,
- $j = 5, \quad q_4 = z_4(t)$ – displacement of masses m_4 and m_{G2} ,
- $j = 6, \quad q_5 = z_5(t)$ – displacement of masses m_{G3} , m_{G4} and m_T .

The generalized coordinates were then used to derive differential equations of forces for the H – G – T model, which is given by:

$$\begin{aligned} j = 1, & \quad m_0 \ddot{z}_0 + (c_0 + c_1) \dot{z}_0 + (k_0 + k_1) z_0 - c_1 \dot{z}_1 - k_1 z_1 = 0 \\ j = 2, & \quad m_1 \ddot{z}_1 + (c_1 + c_2 + c_3) \dot{z}_1 + (k_1 + k_2 + k_3) z_1 - c_1 \dot{z}_0 - k_1 z_0 - c_2 \dot{z}_2 - k_2 z_2 \\ & \quad - c_3 \dot{z}_3 - k_3 z_3 = 0 \\ j = 3, & \quad m_2 \ddot{z}_2 + (c_2 + c_4) \dot{z}_2 + (k_2 + k_4) z_2 - c_2 \dot{z}_1 - k_2 z_1 - c_4 \dot{z}_4 - k_4 z_4 = 0 \\ j = 4, & \quad (m_3 + m_{G1}) \ddot{z}_3 + (c_3 + c_{G1}) \dot{z}_3 + (k_3 + k_{G1}) z_3 - c_3 \dot{z}_1 - k_3 z_1 - c_{G1} \dot{z}_5 - k_{G1} z_5 = 0 \\ j = 5, & \quad (m_4 + m_{G2}) \ddot{z}_4 + (c_4 + c_{G2}) \dot{z}_4 + (k_4 + k_{G2}) z_4 - c_4 \dot{z}_2 - k_4 z_2 - c_{G2} \dot{z}_5 - k_{G2} z_5 = 0 \\ j = 6, & \quad (m_{G3} + m_{G4} + m_T) \ddot{z}_5 + (c_{G1} + c_{G2}) \dot{z}_5 + (k_{G1} + k_{G2}) z_5 - c_{G1} \dot{z}_3 - k_{G1} z_3 \\ & \quad - c_{G2} \dot{z}_4 - k_{G2} z_4 = F(t) \end{aligned} \quad (2)$$

For the second condition, when the operator is working without the anti-vibration glove, i.e. for the model of the system consisting of the human operator and the tool (H – T), the generalized coordinates are as follows:

- $j = 1, q_0 = z_0(t)$ – displacement of mass m_0 ,
- $j = 2, q_1 = z_1(t)$ – displacement of mass m_1 ,
- $j = 3, q_2 = z_2(t)$ – displacement of mass m_2 ,
- $j = 4, q_3 = z_3(t)$ – displacement of masses m_3, m_4 and m_T .

The number of generalized coordinates is smaller since the model of the anti-vibration glove (enclosed by dotted line in Fig. 2) is not included. As a result, masses m_3 and m_4 are in direct contact with mass m_T , which is a substitute for the tool. The exclusion of the glove model eliminates two points of reduction from model (2), i.e. $j = 4$ and $j = 5$. Consequently, the mathematical model of the biomechanical system with 4 degrees of freedom can be expressed as:

$$\begin{aligned}
 j = 1, & \quad m_0 \ddot{z}_0 + (c_0 + c_1) \dot{z}_0 + (k_0 + k_1) z_0 - c_1 \dot{z}_1 - k_1 z_1 = 0 \\
 j = 2, & \quad m_1 \ddot{z}_1 + (c_1 + c_2 + c_3) \dot{z}_1 + (k_1 + k_2 + k_3) z_1 - c_1 \dot{z}_0 - k_1 z_0 - c_2 \dot{z}_2 - k_2 z_2 \\
 & \quad - c_3 \dot{z}_3 - k_3 z_3 = 0 \\
 j = 3, & \quad m_2 \ddot{z}_2 + (c_2 + c_4) \dot{z}_2 + (k_2 + k_4) z_2 - c_2 \dot{z}_1 - k_2 z_1 - c_4 \dot{z}_3 - k_4 z_3 = 0 \\
 j = 4, & \quad (m_3 + m_4 + m_T) \ddot{z}_3 + (c_3 + c_4) \dot{z}_3 + (k_3 + k_4) z_3 - c_4 \dot{z}_2 - k_4 z_2 \\
 & \quad - c_3 \dot{z}_1 - k_3 z_1 = F(t)
 \end{aligned} \tag{3}$$

The next step involved assessing the effect of vibrations on the human body in terms of energy, which consists in determining three components of energy inputs, associated with three kinds of structural forces: inertial, dissipative and elastic. This was achieved by applying the First Principle of Power Distribution in a Mechanical System [1, 2]. The components of energy were calculated using numerical simulations, i.e. by determining energy inputs flowing through the dynamic structure of the H – G – T system. Specific energy inputs absorbed by the human body were calculated as integrals of the absolute values of structural forces. In this way, it is possible to define and compare the flow of energy through the human body under both conditions, i.e. when using the tool with and without the glove. Values of component energy inputs in the dynamic structure of the human body, defined as a sum of energy inputs due to specific types of forces at all point of reduction, were defined as follows:

- the energy component due to inertial forces for the human operator working without the glove:

$$E_{H-INE,t} = \int_0^t |m_0 \ddot{z}_0 \dot{z}_0| dt + \int_0^t |m_1 \ddot{z}_1 \dot{z}_1| dt + \int_0^t |m_2 \ddot{z}_2 \dot{z}_2| dt + \int_0^t |(m_3 + m_4) \ddot{z}_3 \dot{z}_3| dt \tag{4}$$

- the energy component due to dissipative forces for the human operator working without the glove:

$$E_{H-DIS,t} = \int_0^t |(c_0 + c_1) \dot{z}_0|^2 dt + \int_0^t |(c_1 + c_2 + c_3) \dot{z}_1|^2 dt + \int_0^t |(c_2 + c_4) \dot{z}_2|^2 dt + \int_0^t |(c_3 + c_4) \dot{z}_3|^2 dt \tag{5}$$

- the energy component due to elastic forces for the human operator working without the glove:

$$E_{\text{H-ELA},t} = \int_0^t |(k_0 + k_1)z_0\dot{z}_0| dt + \int_0^t |(k_1 + k_2 + k_3)z_1\dot{z}_1| dt + \int_0^t |(k_2 + k_4)z_2\dot{z}_2| dt + \int_0^t |(k_3 + k_4)z_3\dot{z}_3| dt \quad (6)$$

For the condition with the anti-vibration glove, energy components are given as follows:

- the energy component due to inertial forces for the human operator working with the glove:

$$E_{\text{H+G-INE},t} = \int_0^t |m_0\ddot{z}_0\dot{z}_0| dt + \int_0^t |m_1\ddot{z}_1\dot{z}_1| dt + \int_0^t |m_2\ddot{z}_2\dot{z}_2| dt + \int_0^t |m_3\ddot{z}_3\dot{z}_3| dt + \int_0^t |m_4\ddot{z}_4\dot{z}_4| dt \quad (7)$$

- the energy component due to dissipative forces for the human operator working with the glove:

$$E_{\text{H+G-DIS},t} = \int_0^t |(c_0 + c_1)\dot{z}_0^2| dt + \int_0^t |(c_1 + c_2 + c_3)\dot{z}_1^2| dt + \int_0^t |(c_2 + c_4)\dot{z}_2^2| dt + \int_0^t |c_3\dot{z}_3^2| dt + \int_0^t |c_4\dot{z}_4^2| dt \quad (8)$$

- the energy component due to elastic forces for the human operator working with the glove:

$$E_{\text{H+G-ELA},t} = \int_0^t |(k_0 + k_1)z_0\dot{z}_0| dt + \int_0^t |(k_1 + k_2 + k_3)z_1\dot{z}_1| dt + \int_0^t |(k_2 + k_4)z_2\dot{z}_2| dt + \int_0^t |k_3z_3\dot{z}_3| dt + \int_0^t |k_4z_4\dot{z}_4| dt \quad (9)$$

Simulations were implemented in MATLAB/simulink R2009a, using the ode113 (Adams) solver, with integration steps ranging from a minimum of 0.00001 to a maximum of 0.0001 second, and a tolerance of 0.001. Simulations were performed for two periods, i.e. $t_1 = 5$ and $t_2 = 30$ seconds. In order to exclude the impact of unsteady motion during startup on the value of the final energy input used for comparative analysis, it was calculated as a difference between energy input values after time t_2 and t_1 . Results obtained for the two methods are analysed, interpreted and compared in the second part of the article.

4. Summary

The main outcome of the work undertaken in this part of the study is the formulation of a discrete model of the anti-vibration glove, which was used in experimental tests. In addition, the vibration acceleration signal generated by the motion of the working grinder and affecting the operator was modelled – Fig.1.

Performance results obtained during tests demonstrated that the application of the anti-vibration glove increased vibrations of the grinder, as indicated by higher RMS values of vibration accelerations measured at the handle – Table 1.

The first part of the study was only the starting point for the second part, in which we compare results obtained by applying the two methods mentioned above. Results of comparative analysis are presented in the second part: “*Assessment of the effectiveness of anti-vibration gloves. A comparison of the conventional and energy-based method. Analysis and interpretation of results – part two.*”

Acknowledgements

The study was financed from a grant awarded by the Ministry of Science and Higher Education for the research project no. 02/21/DSMK/3501.

References

1. M. W. Dobry, *Optymalizacja przepływu energii w systemie Człowiek – Narzędzie – Podłoże (CNP)*, Politechnika Poznańska, Poznań 1998.
2. M. W. Dobry, *Podstawy diagnostyki energetycznej systemów mechanicznych i biomechanicznych*, Wydawnictwo Naukowe Instytutu Technologii Eksploatacji – PIB, Radom 2012.
3. R. G. Dong, J. H. Dong, J. Z. Wu, S. Rakheja, *Modeling of biodynamic responses distributed at the fingers and the palm of the human hand–arm system*, *Journal of Biomechanics*, **40** (2007) 2335 – 2340.
4. R. G. Dong, S. Rakheja, T. W. McDowell, D. E. Welcome, J. Z. Wu, *Estimation of the biodynamic responses distributed at fingers and palm based on the total response of the hand-arm system*, *International Journal of Industrial Ergonomics*, **40** (2010) 425 – 436.
5. R. G. Dong, D. E. Welcome, T. W. McDowell, J. Z. Wu, *Modeling of the biodynamic responses distributed at the fingers and palm of the hand in three orthogonal directions*, *Journal of Sound and Vibration*, **332** (2013) 1125 – 1140.
6. M. J. Griffin, *Handbook of Human Vibration*, Academic Press, London 1990.
7. G. Meltzer, *A Vibration Model for the Human Hand-Arm-System*, *Studies in Environmental Science*, **13** (1981) 210 – 221.
8. D. D. Reynolds, *Hand-arm vibration: A review of three years' research*, in: *Proceedings of the 3rd International Hand-Arm Vibration Conference*, Ohio, USA, (1977) 99 – 129.
9. ISO 10068:2012, *Mechanical vibration and shock - Mechanical impedance of the human hand-arm system at the driving point*.

10. PN-EN ISO 10819:2000, *Drgania i wstrząsy mechaniczne. Drgania oddziałujące na organizm człowieka przez kończyny górne. Metoda pomiaru i oceny współczynnika przenoszenia drgań przez rękawice na dłoń operatora.*
11. PN-EN ISO 10819:2013-12, *Drgania i wstrząsy mechaniczne. Drgania oddziałujące na organizm człowieka przez kończyny górne. Pomiar i ocena współczynnika przenoszenia drgań przez rękawice na dłoń operatora.*

Assessment of the Effectiveness of Anti-Vibration Gloves. A Comparison of the Conventional and Energy Method. Analysis and Interpretation of Results – Part Two

Tomasz HERMANN

*Poznan University of Technology, Institute of Applied Mechanics
Jana Pawła II 24, Poznan, tomasz.hermann@put.poznan.pl*

Marian Witalis DOBRY

*Poznan University of Technology, Institute of Applied Mechanics
Jana Pawła II 24, Poznan, marian.dobry@put.poznan.pl*

Abstract

The article is the second part of the article entitled “Assessment of the effectiveness of anti-vibration gloves. A comparison of the conventional and energy method. Introduction – part one” [4], which presents the assumptions and the construction of models of the biodynamic system consisting of the human operator, the anti-vibration glove and the hand-held power tool. The second part is devoted to a comparative analysis and interpretation of results obtained by means of the two methods. The analysis reveals a positive effect of the anti-vibration glove as a personal protective equipment, which reduces the operator’s exposure to vibrations generated by the angle grinder. However, the effectiveness of the glove was assessed differently by the conventional or the energy method. It was also found that the energy method was a better tool for analyzing the impact of vibrations at different phases of the tool’s operation.

Keywords: biomechanical system, local vibrations, energy assessment method

1. Introduction

There are a number of factors that need to be taken into account when conducting studies of the effectiveness of vibration reduction of anti-vibration gloves. One of them is the type of hand-held power tool [5]. In this particular case, the effectiveness of vibration reduction by means of an anti-vibration glove depends, among other things, on the grip force and the pressure exerted by the operator on the tool handle, the vibration acceleration signal generated by the tool, frequency characteristics of the glove’s transmissibility, operating conditions, the mode of operation, the technological process and dynamic properties of an individual operator [3, 5, 6].

Safety requirements for anti-vibration gloves are specified in relevant industrial standard [8]. However, the effectiveness of anti-vibration gloves is assessed in two frequency ranges: mean values of corrected transmissibility for the glove must not exceed 0.9 for the lower frequency range (25 ÷ 200 Hz) and 0.6 for the higher frequency range (200 ÷ 1250 Hz). Only when transmissibility values are lower than or equal to the minimum values can a glove be regarded as an anti-vibration glove [8]. The anti-vibration gloves tested in the study satisfied the safety requirements specified for this kind of personal protective equipment.

The purpose of the study was to determine the difference in the assessment of the effectiveness of vibration reduction depending on the method used, i.e. the conventional and energy method. The methods rely on different assessment criteria: the first case only accounts for vibration accelerations; the second takes into considerations values of energy inputs absorbed by the human body. As a result of the analysis, it was possible to determine the factor change in the assessment of the glove's effectiveness depending on the method used. Based on these values, the two methods were compared in order to identify differences in their assessments.

2. Results of the conventional analysis

Tables 1 and 2 present theoretical and experimental RMS values of vibration accelerations obtained for the condition of working with and without the anti-vibration glove. Results of numerical simulations were obtained by solving mathematical models (2) and (3), presented in the first part of the article [4].

It should be noted that theoretical values of RMS values of vibration accelerations obtained for both conditions were very similar to the mean experimental value – a difference of less than 1%. The results obtained for a new model of the glove (Table 2 in article [4]) represent the first attempt of using dynamic parameters which were determined experimentally. The high degree of similarity is thanks to the new model of the glove, which was adjusted to specific laboratory conditions in which the performance test was conducted.

Table 1. RMS values of vibration accelerations in the case of working without the glove and the difference relative to the mean measured value

Reduction point	Simulated RMS value of vibration accelerations [m/s ²]	Experimental RMS value of vibration accelerations [m/s ²]	Difference relative to the mean experimental value[%]
$j = 4$, mass m_3 and m_4	101.20	101.00 ± 2.82	0.20
$j = 3$, mass m_2	92.46	–	–
$j = 2$, mass m_1	8.99	–	–
$j = 1$, mass m_0	0.12	–	–

Table 2. RMS values of vibration accelerations in the case of working with the glove and the difference relative to the mean measured value

Reduction point	Simulated RMS value of vibration accelerations [m/s ²]	Experimental RMS value of vibration accelerations [m/s ²]	Difference relative to the mean experimental value[%]
$j = 6$, mass m_{G3} , m_{G4} and m_T	117.80	117.00 ± 6.79	0.68
$j = 5$, mass m_4 and m_{G2}	26.76	–	–
$j = 4$, mass m_3 and m_{G1}	26.59	26.55 ± 0.83	0.15
$j = 3$, mass m_2	26.88	–	–
$j = 2$, mass m_1	2.72	–	–
$j = 1$, mass m_0	0.04	–	–

The effectiveness of the anti-vibration glove can be assessed conventionally on the basis of experimental results. In this case, effectiveness is assessed in terms of a dimensionless index, defined as a ratio of the RMS value of vibration accelerations measured at the grinder handle (equivalent to the RMS value experienced by the operator at the palm of the hand without a glove) to the RMS value of vibration accelerations experienced by the operator at the palm of the hand with the glove. The relationship is given by the following formula:

$$I_E = \frac{a_{\text{RMS,H}}}{a_{\text{RMS,P}}} \quad (1)$$

where:

- $a_{\text{RMS,H}}$ – mean RMS value of vibration accelerations at the grinder handle, without the glove, i.e. for $j = 4$, and equal to 101.00 m/s^2 , (Tab. 1),
 $a_{\text{RMS,P}}$ – mean RMS value of vibration accelerations at the palm of the hand, with the glove, i.e. for $j = 4$, and equal to 26.55 m/s^2 (Tab. 2).

By applying this index, the effectiveness of the anti-vibration glove can be expressed as a factor change, which was equal to 3.80. This means that the tested glove reduces the RMS value of vibration accelerations relative to the value obtained when the glove is not used. In this case, the glove reduces the transmission of vibrations, i.e. reduces accelerations of vibrations by a factor of 3.80.

The high factor change in the effectiveness of protection is mainly due to the measurement of RMS values of vibration accelerations, which were measured under the linear weighting setting, i.e. without any filters and for the measurement frequency range between 10 and 10,000 Hz. This setting was necessitated by the requirements concerning input data for energy analysis. Additional series of measurements were performed using the H/A filter under the same laboratory conditions (Table 3)

Table 3. RMS values of vibration accelerations measured with the H/A filter and linear weighting – laboratory measurements

Measurement condition	Value		Unit
	with H/A filter	with filters	
at the handle (without the glove)	4.15 ± 0.13	101.00 ± 2.82	m/s^2
at the handle (with the glove)	3.75 ± 0.15	117.00 ± 6.79	
at the palm of the hand (with the glove)	2.20 ± 0.03	26.55 ± 0.83	

It should be noted that measurements performed with the H/A filter and without filters (with linear weighting) differ considerably. The results indicate two important facts. First of all, the application of the filter affects the RMS values of vibrations accelerations measured at the tool handle: the RMS value of vibrations accelerations at the handle increases, but only when measured without filters in the linear range between 10 and 10,000 Hz. This means that the anti-vibration glove amplifies vibrations accelerations, but mostly those that are not included in the frequency range specified in the standard, i.e. above 1250 Hz. In the second frequency range, i.e. with the H/A filter, a significant

reduction in vibrations accelerations at the handle was recorded, and this is precisely the value that is relevant in assessing the impact of vibrations generated by tools on the human body.

The second fact that can be concluded from the measurement results is the lower effectiveness of the glove when the H/A filter is used. In this case, the factor change, calculated according to formula (1), is equal to 1.89. The tested glove reduces the RMS of vibrations accelerations in the H/A range, but the reduction of vibrations in the range which is relevant for the human body is lower than the factor change for the wider frequency band.

In summary, the conventional method indicates a positive effect of using the anti-vibration glove for both kinds of measurements. However, the conventional (amplitude-based) method can only be used to compare two conditions: when the operator is working without and with the glove. More information about the effect of vibrations on the human body can be obtained by applying the energy method, which described in the following section.

3. Results of the energy method

Given known dynamic parameters of the model of the human body [7] and measured and simulated RMS values of vibration accelerations obtained by applying the model of the combined H – G – T system, it is possible to conduct energy analysis [1, 2]. The following method can be used to determine the energy input absorbed by a specific subsystem of the H – G – T system, taking into account the impact of the other subsystems. This can be done by identifying the energy component associated with the human body subsystem, which is part of the combined model.

In order to determine the energy input absorbed by the human body, it is necessary to identify energy components (energy inputs) of three kinds of forces, according to formulas (4)–(9), presented in the first part of the article [4]. This task was accomplished by performing numerical simulations of accelerations, velocity and displacements of vibration associated with structural forces during the operation of the H – G – T system. Results of these simulations are the input for the energy method. Tables 4 and 5 present the results of energy analysis for the condition without and with the anti-vibration glove.

Table 4. Values of energy components of forces (energy inputs) for the model of the operator working without the glove at time $t_1 = 5$ and $t_2 = 30$ seconds

Energy component of forces	Time $t_1 = 5$ seconds [J]	Time $t_2 = 30$ seconds [J]	Difference $E_{C-X,t_2} - E_{C-X,t_1}$ [J]
inertial $E_{H-INE,t}$	2.58	15.32	12.74
dissipative $E_{H-DIS,t}$	9.66	57.61	47.95
elastic $E_{H-ELA,t}$	11.77	43.36	31.59
Σ	24.01	116.29	92.28

Table 5. Values of energy components of forces (energy inputs) for the model of the operator working with the glove at time $t_1 = 5$ and $t_2 = 30$ seconds

Energy component of forces	Time $t_1 = 5$ seconds [J]	Time $t_2 = 30$ seconds [J]	Difference $E_{C+R-X,t_2} - E_{C+R-X,t_1}$ [J]
inertial $E_{H+G-INE,t}$	0.22	1.27	1.05
dissipative $E_{H+G-DIS,t}$	0.92	5.23	4.31
elastic $E_{H+G-ELA,t}$	3.32	6.29	2.97
Σ	4.46	12.79	8.33

Figure 1 shows a comparison of the sum of three energy components associated with 3 kinds of forces – inertial, dissipative and elastic – for the model of the operator working without and with the glove. The numbers represent energy values after two periods: $t_1 = 5$ seconds and $t_2 = 30$ seconds. The third section of the chart shows the difference between the two values in order to exclude the energy input absorbed by the human body during the unsteady motion in the startup of the system.

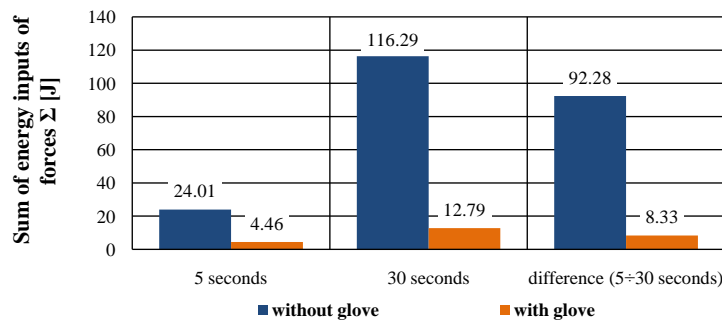


Figure 1. Sums of energy components of forces for the model of the operator working without and with the glove after time $t_1 = 5$ seconds and $t_2 = 30$ seconds and in the interval between t_2 and t_1 , i.e. during the steady motion phase ($E_{X,t_2} - E_{X,t_1}$)

The results presented in Figure 1 indicate that the anti-vibration glove reduces the energy input absorbed by the human body. Under this approach, the effectiveness of the glove is also measured in terms of a dimensionless index, which is defined as a ratio of the sum of three energy components of forces for the model of the operator working without the glove to the corresponding sum calculated for the case with the glove. The index is expressed by the following formula:

$$E_C = \frac{E_{H-INE,t} + E_{H-DIS,t} + E_{H-ELA,t}}{E_{H+G-INE,t} + E_{H+G-DIS,t} + E_{H+G-ELA,t}} \tag{2}$$

where:

$E_{H-X,t}$ – energy components associated with inertial, dissipative and elastic forces for the case without the glove and calculated using formulas (4)–(6) presented in the first part of the article [4],

$E_{H+G-X,t}$ – energy components associated with inertial, dissipative and elastic forces for the case with the glove, calculated using formulas (7)–(9) presented in the first part of the article [4].

It is worth noting that the effectiveness of the glove is different for each of the three situations. After calculating the value of the effectiveness index, the following order was obtained:

- after $t_1 = 5$ seconds – a factor change of 5.38,
- after $t_2 = 30$ seconds – a factor change of 9.09,
- in the interval between 5 and 30 seconds, during the steady motion – a factor change of 11.08.

It should be emphasized that the effectiveness of the glove increases as the time of operation increases. The startup phase is particularly critical: after $t_1 = 5$ seconds the index of effectiveness of is the lowest and is equal to 5.38. One practical recommendation that can be derived from this fact is that the tool should not be restarted repeatedly within a short interval of time.

After a longer period of time ($t_2 = 30$ seconds), the input of vibration energy absorbed by the operator working with the glove is considerably lower. This is because the flow of vibration energy absorbed by the body is lower by a factor of more than 9. This means that the most optimal phase for using the tool is the period of steady motion. This is also confirmed by the value of the effectiveness index calculated for the interval between 5 and 30 seconds: in this case the vibration energy input is reduced by a factor of over 11.

Figure 2 presents a structural distribution of energy inputs in the human body associated with the three kinds of forces. The percentage share of each energy component was calculated by relating the energy input associated with the specific force to the total energy input absorbed by the human body. Once again, the resulting values are shown for three situations: after time $t_1 = 5$ and $t_2 = 30$ seconds and in the interval between 5 and 30 seconds (for the steady motion). The structural distribution is calculated using the following formula:

$$P_S = \frac{E_{X,t}}{E_{X-INE,t} + E_{X-DIS,t} + E_{X-ELA,t}} \cdot 100\% \quad (3)$$

where:

$E_{X,t}$ – values of energy components (energy inputs) of inertial, dissipative and elastic forces for each of the three situations (values from Tables 4 and 5).

The results shown in Figure 2 indicate that the percentage share of structural energy inputs associated with the three forces for the operator working without and with the glove depends on the period of time. This is an important conclusion since the structural energy inputs can be linked with specific changes in the human body [1, 2].

When the tool is used for a short period of time, the percentage share of energy input due to elastic forces for both conditions is the highest – Fig. 2a. For this reason, this energy component will mainly affect the elastic parts of the human body, which include muscles, tendons and joint capsules. As a result, repeated restarts of the grinder within a short period of time will increase the likelihood of pathological changes in these body parts.

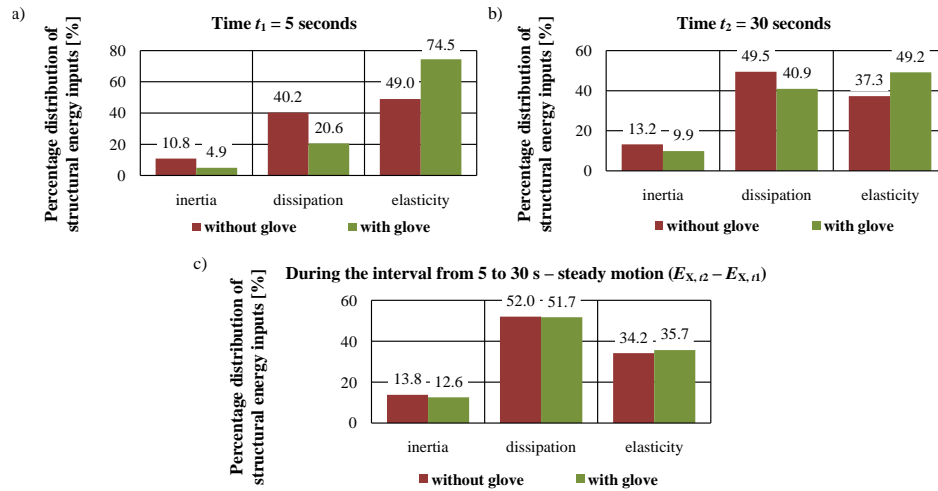


Figure 2. Percentage share of structural energy components for the model of the operator working with and without the glove: a) after $t_1 = 5$ seconds; b) after $t_2 = 30$ seconds c) during the interval from 5 to 30 seconds – steady motion ($E_{X,t2} - E_{X,t1}$)

The distribution changes for the longer period $t_2 = 30$ seconds. In this case, for the case of working without the tool, the dominant energy component is associated with dissipative forces, while for the case with the glove, the energy input from elastic forces – Fig. 2b. However, this conclusion is somewhat misleading because the contributions are affected by the energy inputs generated during the unsteady motion, shown in Fig.1. When one analyses the structural distribution of energy inputs in the interval of steady motion, shown in Figure 2c, one can see that for both conditions the dominant energy input is associated with dissipative forces, which can be linked to an increase in body temperature caused by the dissipation of energy.

4. Comparison of the conventional and the energy method

The two methods should be compared on the basis of linear measurements obtained for the frequency range of 10 to 10000 Hz. For this frequency range, the effectiveness of the glove, according to the conventional (amplitude-based) method is equal to 3.80. When the effectiveness is assessed in terms of energy, it should be based on value obtained for the steady motion, which is 11.08. This choice is motivated by the fact that the measurements of RMS values of vibration accelerations were made during the steady motion of the tool.

5. Summary

The main outcome of the study is that, regardless of the method used, the anti-vibration glove was found to be effective in reducing the impact of vibrations generated by the tool. However, a different degree of effectiveness was obtained for each method: in the case of the conventional method (based on amplitude values), it was 3.80, while for

the energy method, it was 11.08. As can be seen from the data, the assessment of effectiveness is evidently different.

The study has also shown the energy method to be a more holistic approach to analyzing the effect of vibrations on the human body. In particular, the energy analysis has revealed the significant contribution of vibration energy absorbed by the human body during the startup phase – Fig. 1. It was also possible to notice that the impact of vibrations changes depended on the time of using the tool – Fig. 2 – from the startup of the biomechanical system to the steady motion phase. Based on energy simulations, it can be concluded that exposure to vibrations generated by angle grinders can, first of all, lead to pathological changes in the elastic elements of the operator or to overheating, and only to a lesser degree can disrupt blood flow.

Comparative studies in this areas will be continued. The analysis described in the article is also the first attempt at building a medium-sized discrete model of an anti-vibration glove specially designed for use with an angle grinder. Dynamic parameters of the glove will be determined along the three directions of vibrations, i.e. along the x , y and z axes.

Acknowledgements

The study was financed from a grant awarded by the Ministry of Science and Higher Education for the research project no. 02/21/DSPB/3494.

References

1. M. W. Dobry, *Optimalizacja przepływu energii w systemie Człowiek - Narzędzie - Podłoże (CNP)*, Politechnika Poznańska, Poznań 1998.
2. M. W. Dobry, *Podstawy diagnostyki energetycznej systemów mechanicznych i biomechanicznych*, Wydawnictwo Naukowe Instytutu Technologii Eksploatacji – PIB, Radom 2012.
3. Z. Engel, W. M. Zawieska, *Hałas i drgania w procesach pracy: źródła, ocena, zagrożenia*, Centralny Instytut Ochrony Pracy – Państwowy Instytut Badawczy (CIOP-PIB), Warszawa 2010.
4. T. Hermann, M. W. Dobry, *Assessment of the effectiveness of anti-vibration gloves. A comparison of the conventional and energy method. Introduction – part one*, Vibrations in Physical Systems, **28** (2017).
5. J. Koton, J. Szopa, *Rękawice antywibracyjne – ocena skuteczności i zasady doboru do stanowisk pracy*, Bezpieczeństwo Pracy. Nauka i Praktyka, **11** (1999) 2 – 5.
6. D. Koradecka (edytor), *Bezpieczeństwo i higiena pracy*, Centralny Instytut Ochrony Pracy – Państwowy Instytut Badawczy (CIOP-PIB), Warszawa 2008.
7. ISO 10068:2012, *Mechanical vibration and shock. Mechanical impedance of the human hand-arm system at the driving point*.
8. PN-EN ISO 10819:2013-12, *Drgania i wstrząsy mechaniczne. Drgania oddziałujące na organizm człowieka przez kończyny górne. Pomiar i ocena współczynnika przenoszenia drgań przez rękawice na dłoń operatora*.

Dynamic Analysis of Optimized Two-Phase Auxetic Structure

Eligiusz IDCZAK

*Institute of Applied Mechanics, Poznan University of Technology
ul. Jana Pawla II 24, 60-965 Poznan, Poland
eligiusz.j.idczak@doctorate.put.poznan.pl*

Tomasz STREK

*Institute of Applied Mechanics, Poznan University of Technology
ul. Jana Pawla II 24, 60-965 Poznan, Poland
tomasz.strek@put.poznan.pl*

Abstract

This paper presents a dynamic analysis of earlier optimized auxetic structure. This optimization based on the distribution of two materials in such way to obtain a minimal value of Poisson's ratio (PR), which indicates the auxetic properties. The initial optimized shape was so-called star structure, which if is made from one material has the PR close to 0.188. After optimization with the goal function of PR-minimization, the obtained value was equal to -9.5043. Then the eigenfrequencies for the optimized structure were investigated. The calculations were carried out by means of Finite Element Method (FEM). For optimization of the value of Poisson's ratio was used algorithm MMA (Method of Moving Asymptotes). The computing of single material properties (PR, Young's modulus, density) for the whole shape was made by means of SIMP method (Solid Isotropic Method with Penalization).

Keywords: negative PR, auxetics, eigenfrequency, topology optimization, dynamic analysis

1. Introduction

Dynamic analysis is one of the most important parts of investigations of structures and constructions. It allows evaluating their real behaviours under influence of real forces. The carrying out of dynamic simulations is mainly important during the first step of the design process to find out how the newly designed structure or shape will behave under dynamic exerting forces.

The first step for dynamic analysis is computing of eigenfrequencies. Natural frequencies are the frequencies at which a system tends to oscillate in the absence of any driving or damping force. The calculating of eigenfrequencies allows checking how the structure will behave after load and how will cooperate with other elements of the system. It is the initial stage of the checking the usefulness of the shape for the industrial applications.

The most common auxetic metamaterials are cell structures which are consisted of many repeated single cells. These structures are constantly developed because of their advantageous properties like low density, beneficial damping behaviour, energy absorption and many others. The examples of auxetic cellular metamaterials are: re-entrant honeycombs (Fig. 1), rotating units (Fig. 2.), star-shaped structures (Fig. 3.), "missing rib" (Fig. 4.) "double arrowhead" (Fig. 5.), chiral and anti-chiral structures (Fig. 6.).

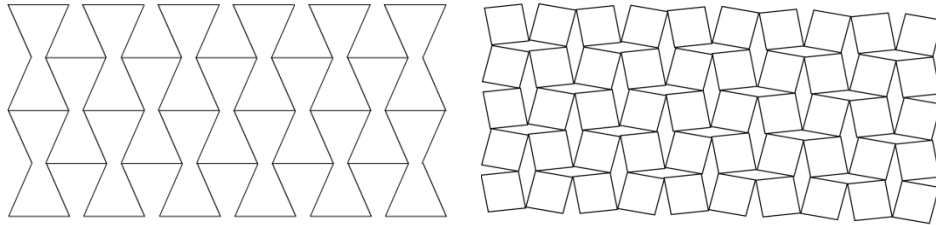


Figure 1. Re-entrant honeycomb $\nu = -0.39$ [1] Figure 2. Rotating squares $\nu = -0.963$ [2]

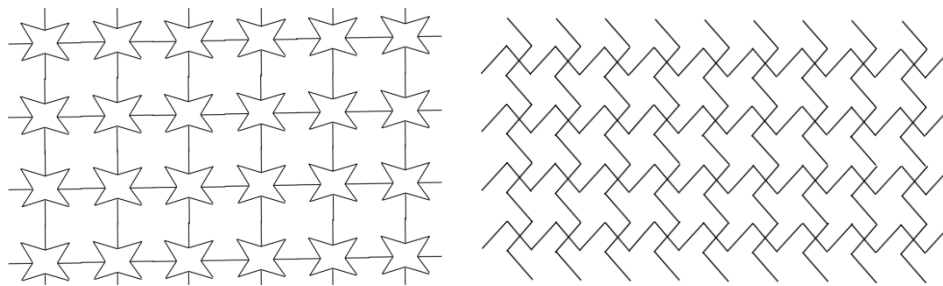


Figure 3. Star structure $\nu = -0.25 \div -0.35$ [3] Figure 4. Missing rib structure $\nu = -0.6$ [4]

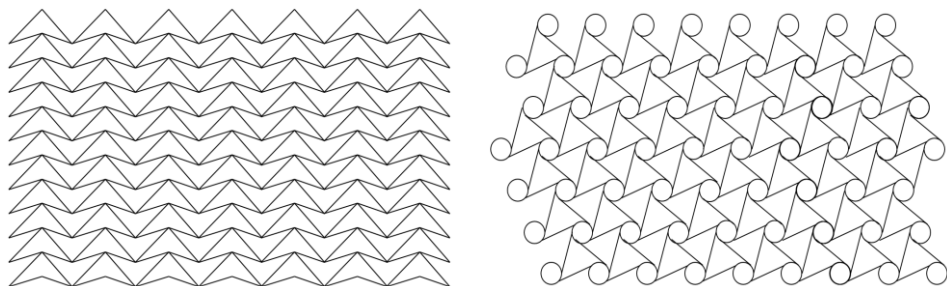


Figure 5. Double arrow head topology

Figure 6. Chiral honeycomb $\nu = -0.98$ [5]

As presented above the values of negative PR for homogenous cellular structures is not less than -1. But through material distribution by means of topology optimization, the two-phase auxetic cell can have the value of PR on the level -9.5.

In the literature, there are many examples of dynamic analysis of auxetics. First works about deformation mechanism of structures with negative PR were presented by Gibson [6] and the inventor of name “auxetic” - R. Lakes in his papers [7-9]. Scarpa [10] shows various dynamic characteristics of open cell compliant polyurethane foam with auxetic behavior. In the works [11, 12] was shown the dynamic analysis of periodic auxetic chiral structures. The authors numerically and experimentally proved that the chiral structures deform when were excited at one of its eigenfrequencies. This is particularly important

because resonance can be used to minimize the power required for the occurrence of localized deformations.

The most common analysis is connected with simulations and experiments which confirm whether the structures with negative PR have favourable properties for damping the vibrations or acoustic isolations. It is also defined the specific ratios for checking the damping's properties like VTL (Vibration Transmission Loss) or STL (Sound Transmission Loss) [13-15]. The natural frequencies for the earlier optimized structure with the criterion of minimal internal energy were described in the papers [16, 24].

The auxetics are also checked to find out which deformation will take place under influence of harmonic loading force and to compute the value of crushing strength of the structure. Dynamic comparing analysis of re-entrant honeycomb (negative PR) and hexagonal honeycomb (positive PR) proves the relation between negative PR and crushing strength [17].

The dynamic behaviour of the composite with auxetic core is presented in work [18]. Authors presented effective properties and dynamic response of a sandwich panel made of two face sheets and core.

Other optimized shapes with the goal function of minimization of the Poisson's ratio were shown in the papers [22, 23].

2. Properties and methods

To compute the effective values of parameters (Young's modulus, Poisson's ratio, density) of the two-phase shape cell is used effective interpolation method. Here it's used the solid isotropic material with a penalization (SIMP) scheme. The most important part of SIMP is the insertion of an interpolation function as a function of the continuous variable. This interpolation function defines the mechanical properties. The particular parameters in SIMP method for the minimization of PR fulfill the equations:

$$E(r) = E_1 + (E_2 - E_1)r^p \quad (1)$$

$$\nu(r) = \nu_1 + (\nu_2 - \nu_1)r^p \quad (2)$$

where: $r = r(x)$ – control variable for computing the effective values of properties, p – penalization parameter, which in optimizations is equal to 3 (previous works about SIMP recognize penalization parameter equal to 3 as the most effective), E_1, E_2, ν_1, ν_2 – Young's moduli and Poisson's ratios of first and second material. Density of material represents continuous variable $0 < r < 1$. In this method, the continuous variables are described as material densities. SIMP also can evaluate bulk and shear moduli and other physical properties.

The Poisson's ratio for the homogenous, isotropic elastic solid material is the negative ratio of transverse to longitudinal strain at every point in a body under longitudinal loading. In a material with two phases where the ratios may be changed classic definition Poisson's ratio isn't possible to use. The new definition of Poisson's ratio was described by many authors and introduces small change to an equation and it is calculated as a negative ratio of the average transverse to longitudinal strains [19]:

$$v_{eff} = -\frac{\overline{\varepsilon_t}}{\overline{\varepsilon_l}} \tag{3}$$

where: $\overline{\varepsilon_t}$ – average transverse strain, $\overline{\varepsilon_l}$ – average longitudinal strain. When the force is applied along the y-axis, the average transverse strain is defined as:

$$\overline{\varepsilon_t} = \frac{\int_{\Gamma_1} u_1 d\Gamma}{L_x \int_{\Gamma_1} d\Gamma} \tag{4}$$

where Γ_1 is the boundary parallel ($x = L_x = 0.4$) to the boundary with prescribed displacement applied. The average longitudinal strain is defined as:

$$\overline{\varepsilon_l} = \frac{\int_{\Gamma_2} u_2 d\Gamma}{L_y \int_{\Gamma_2} d\Gamma} \tag{5}$$

where Γ_2 is the boundary ($y = L_y = 0.4$) where a load is applied.

Because of using SIMP scheme effective Poisson's ratio must be dependent on control variable r, like in the equation (6):

$$v_{eff}(r) = -\frac{\overline{\varepsilon_t(r)}}{\overline{\varepsilon_l(r)}} \tag{6}$$

SIMP scheme for control variable function must have two constraints - pointwise inequality (7) and integral inequality (8), which are given below:

$$0 \leq r(x) \leq 1 \text{ for } x \in S \tag{7}$$

$$0 \leq \int_S r(x) dS \leq A_f \cdot S \tag{8}$$

where: x - defined coordinate, A_f – fraction of the second material of the domain S . The order of optimization order is as follows: FEM – discretization, the redefinition of minimization function with applied constraints and at the end the value of control variable is calculated at every mesh node as:

$$r(x) = \sum_{i=1}^N r_i \cdot \Phi_i(x) \tag{9}$$

where: $\Phi_i(x)$ are the shape functions, i – is the number of an element node, N – is the amount of all nodes.

3. Equation of motion of the solid

The Navier's equation of motion of solid has the form [20]:

$$\rho \frac{\partial^2 \mathbf{u}}{\partial t^2} - \nabla \cdot \boldsymbol{\sigma} = 0 \quad (10)$$

where: \mathbf{u} – the vector of displacements, ρ - the density, $\boldsymbol{\sigma}$ - the stress tensor and is defined as [21]:

$$\boldsymbol{\sigma} = \mathbf{D}\boldsymbol{\varepsilon} = \lambda(\nabla \cdot \mathbf{u})\mathbf{I} + 2\mu\boldsymbol{\varepsilon} \quad (11)$$

where: \mathbf{D} – constitutive matrix, \mathbf{I} – identity matrix, $\boldsymbol{\varepsilon}$ – the strain tensor, defined as:

$$\boldsymbol{\varepsilon} = \frac{1}{2}(\nabla \mathbf{u} + (\nabla \mathbf{u})^T) \quad (12)$$

and μ, λ – Lamé constants, which fulfills the equations:

$$\lambda = \frac{E \cdot \nu}{(1-2\nu)(1+\nu)}, \quad \mu = G = \frac{E}{2(1+\nu)} \quad (13)$$

where: E is Young's modulus, G is shear modulus, ν is Poisson's ratio.

The Navier's equation of motion with linear constitutive relation between stresses and deformations [20] is:

$$\rho \frac{\partial^2 \mathbf{u}}{\partial t^2} - (\mu \nabla^2 \mathbf{u} + (\lambda + \mu) \nabla \nabla \cdot \mathbf{u}) = 0 \quad (14)$$

A harmonic displacement is defined by equation as below:

$$\frac{\partial^2 \mathbf{u}}{\partial t^2} = -\omega^2 \mathbf{u} \quad (15)$$

where: ω – frequency. The displacement vector has the complex form and is defined as:

$$\mathbf{u}(x) = \mathbf{u}_1(x) + i\mathbf{u}_2(x) \quad (16)$$

where the harmonic displacement is a real part of complex form:

$$\mathbf{u}(\mathbf{x}, t) = \text{Re}[\mathbf{u}(\mathbf{x})e^{-i\omega t}] \quad (17)$$

According to aforementioned equations the harmonic equation of motion fulfills the formula:

$$-\rho\omega^2 \mathbf{u} - (\mu \nabla^2 \mathbf{u} + (\lambda + \mu) \nabla \nabla \cdot \mathbf{u}) = 0. \quad (18)$$

4. Numerical results

Optimized star-shape structure with the criterion of minimal PR by means of distribution of two materials is shown in Figure 7 (material 1 – green colour and material 2 – blue colour). Deformation of the compressed structure is presented in Figure 8. The parameters of materials 1 and 2 are presented in Table 2. The minimal effective PR after optimization has the value: -9.5043. The optimization Method of Moving Asymptotes (MMA) and Solid Isotropic Method with Penalization (SIMP) were used to received two-phase structures with lower Poisson's ratio [22].

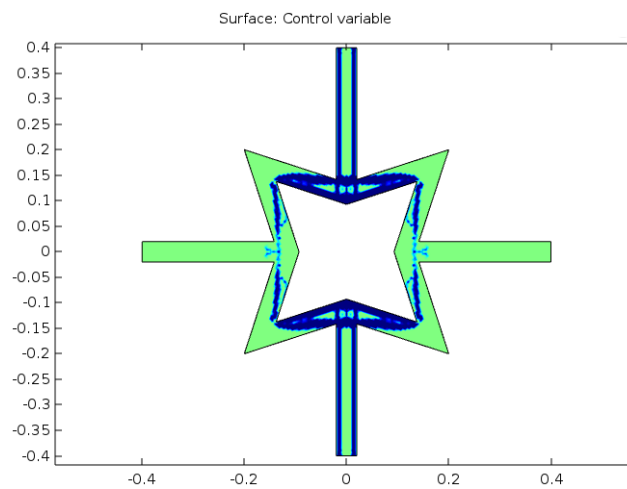


Figure 7. Distribution of two materials in star-shape structure with the minimal PR

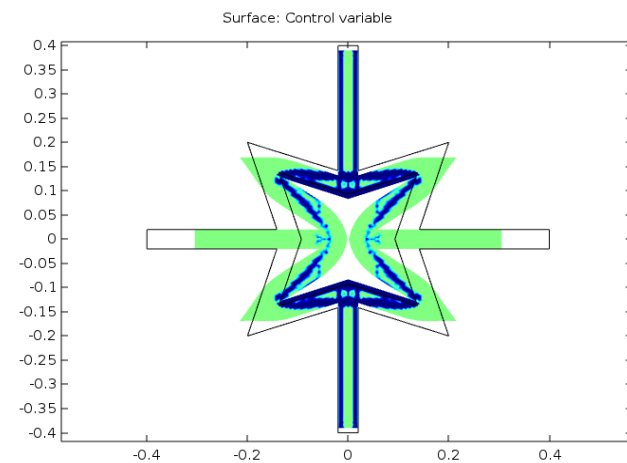


Figure 8. Deformation of structure with minimal PR

Table 1. Material properties of two-phase structure

No.	Material 1	Material 2
Poisson's ratio	0.1	0.33
Young's modulus [MPa]	1e7	1e11

Dynamic analysis of optimized shape consists in the investigation of the deformations after the harmonic load. The seven eigenfrequencies of the structure were determined – in table 2 are the values of each eigenfrequency. To compare the values for two-phase structure presented in table 2, the results for homogenous one-phase structure are also presented. The mode shapes for each natural frequency are shown in the Figures 9-15 (color figures available only online).

Table 2. Values of eigenfrequencies for structures

No. of eigenfrequency		1	2	3	4	5	6	7
Two-phase	Value [Hz]	20.472	55.239	71.912	117.17	151.83	158.53	186
One-phase	Value [Hz]	96.63	351.64	443.02	620.82	800.53	944.99	1088.7

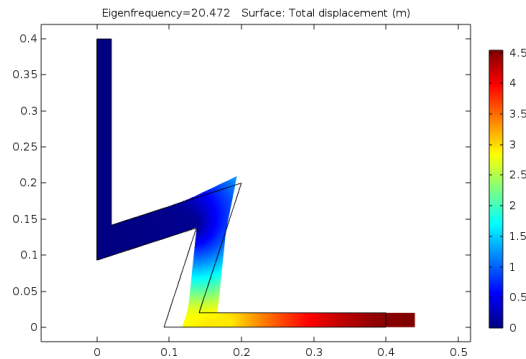


Figure 9. Mode shape for the quarter of optimized structure (eigenfrequency 20.472 Hz)

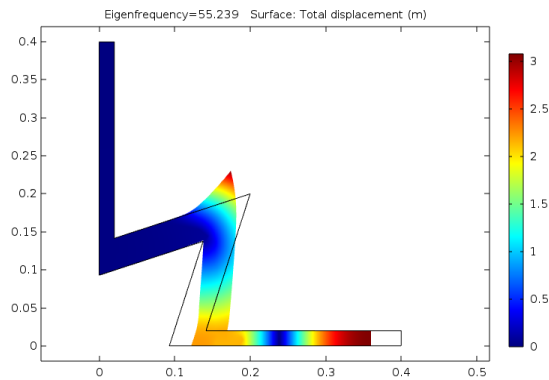


Figure 10. Mode shape for the quarter of optimized structure (eigenfrequency 55.239 Hz)

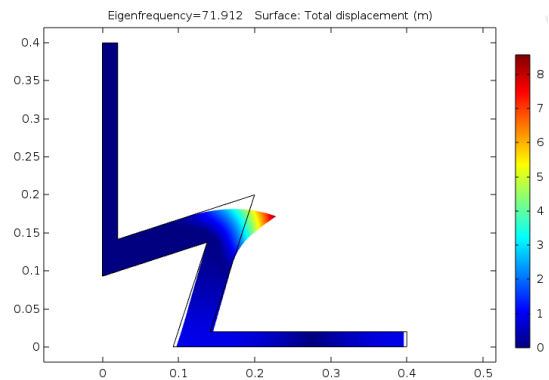


Figure 11. Mode shape for the quarter of optimized structure (eigenfrequency 71.912 Hz)

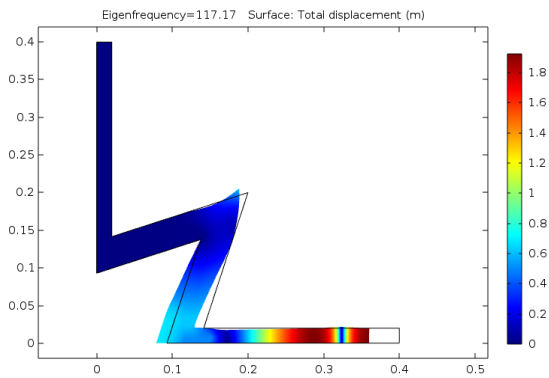


Figure 12. Mode shape for the quarter of optimized structure (eigenfrequency 117.71 Hz)

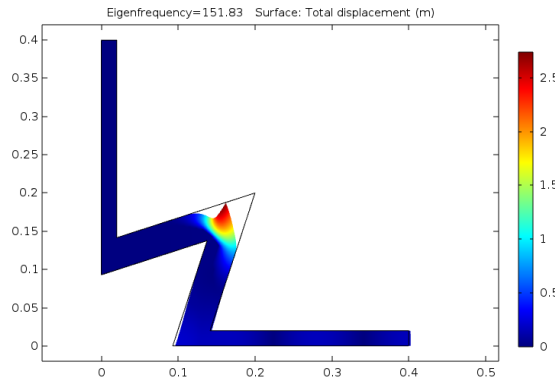


Figure 13. Mode shape for the quarter of optimized structure (eigenfrequency 151.83 Hz)

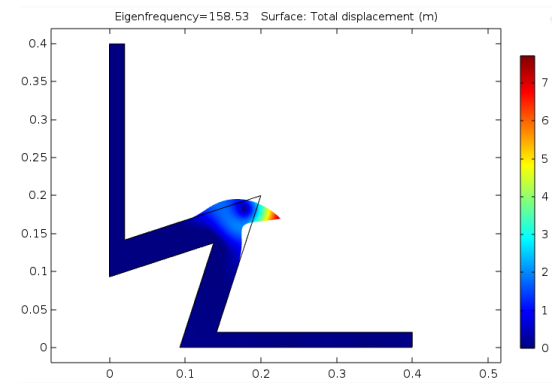


Figure 14. Mode shape for the quarter of optimized structure (eigenfrequency 158.53 Hz)

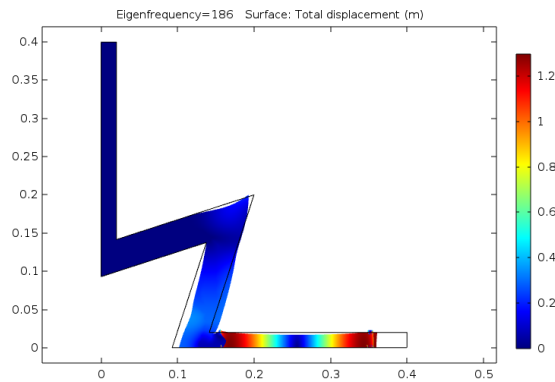


Figure 15. Mode shape for the quarter of optimized structure (eigenfrequency 186 Hz)

5. Conclusions

Dynamic properties of the auxetic structure composed of two materials were investigated. The eigenfrequencies of minimized shape and amplitude of forced vibration were determined.

The knowledge about these dynamic properties can be useful for deciding how serviceable will be the whole structure. In the future may be possible to apply analyzed or similar structure to the industrial applications.

Acknowledgments

This work was supported by grants of the Ministry of Science and Higher Education in Poland: 02/21/DS PB/3493/2017 and 02/21/DSMK/3498/2017. The simulations have been carried out at the Institute of Applied Mechanics, Poznan University of Technology.

References

1. E. A. Friis, R. S. Lakes, J. B. Park, *Negative Poisson's ratio polymeric and metallic foams.*, Science, **23**(12) (1988) 4406 – 4414.
2. M. N. Ali, J. J. C. Busfield, I. U. Rehman, *Auxetic oesophageal stents: structure and mechanical properties*, Journal of Materials Science: Materials in Medicine, **25**(2) (2014) 527 – 553.
3. M. Rad, A. Zaini, A. Amran, *Computational Approach in Formulating Mechanical Characteristics of 3D Star Honeycomb Auxetic Structure*, Advances in Materials Science and Engineering, (2015) 1 – 11.
4. C. W. Smith, J. N. Grima, K. E. Evans *A novel mechanism for generating auxetic behaviour in reticulated foams: missing rib foam model*, Acta Materialia, **48**(17) (2000) 4349 – 4356.
5. A. Alderson, K. L. Alderson, D. Attard, K. E. Evans, K. E. R. Gatt, J. N. Grima, W. Miller, N. Ravirala, C. W. Smith, C. W. K. Zied, *Elastic constants of 3-, 4- and 6-connected chiral and anti-chiral honeycombs subject to uniaxial in-plane loading*, Composites Science and Technology, **70**(7) (2010) 1042 – 1048.
6. L. J. Gibson, M. F. Ashby, *The mechanics of three-dimensional cellular materials*. Proc. R. Soc. A Math. Phys. Eng. Sci., **382** (1982) 43 – 59.
7. R. S. Lakes, *Foam Structures with a Negative Poisson's Ratio*. Science (80-.), **235** (1987) 1038 – 1040.
8. R. S. Lakes, *Deformation Mechanisms in Negative Poisson's Ratio Materials: Structural Aspects*, J. Mat. Sci., **26** (1991) 2287 – 2292.
9. D. Prall, R.S. Lakes, *Properties of a Chiral Honeycomb with Poisson's Ratio of -1*, Int. J. of Mechanical Sciences, **39** (1996) 305–314.
10. F. Scarpa, L. G. Ciffo, J. R. Yates, *Dynamic properties of high structural integrity auxetic open cell foam*. Smart Mater. Struct., **13** (2004) 49 – 56.
11. A. Spadoni, M. Ruzzene, F. Scarpa, *Dynamic response of chiral truss-core assemblies*, Journal of intelligent material systems and structures, **17**(11) (2006) 941 – 952.

12. A. Spadoni, M. Ruzzene, *Structural and Acoustic Behavior of Chiral Trusscore Beams*, Proceedings of the ASME (IMECE 2004) Noise Control and Acoustic Division 2004.
13. H. R. Joshi, *Finite Element Analysis of effective mechanical properties, vibration and acoustic performance of auxetic chiral core sandwich structures*, All Theses., Clemson University, Clemson, South Carolina 2013.
14. R. R Galgalikar, *Design automation and optimization of honeycomb structures for maximum sound transmission loss*, Clemson University, Clemson, South Carolina 2012.
15. E. Idczak, T. Stręk, *Computational Modelling of Vibrations Transmission Loss of Auxetic Lattice Structure*, Vibrations in Physical Systems, **27** (2016) 124 – 128.
16. M. Nienartowicz, T. Stręk, *Finite Element Analysis of Dynamic Properties of Thermally Optimal Two-Phase Composite Structure*, Vibrations in Physical Systems **26** (2014) 203 – 210.
17. W. Liu, M. Wang, T. Luo, Z. Lin, *In-plane dynamic crushing of re-entrant auxetic cellular structure*, Materials & Design, **100** (2016) 84 – 91.
18. T. Strek, H. Jopek, M. Nienartowicz, *Dynamic response of sandwich panels with auxetic cores*, Phys. Status Solidi B, **252**(7) (2015) 1540 – 1550.
19. T. Strek, H. Jopek, K. W. Wojciechowski *The influence of large deformations on mechanical properties of sinusoidal ligament structures*, Smart Materials and Structures, **25**(5) (2016) 05402.
20. B. Lautrup, *Physics of Continuous Matter, Exotic and Everyday Phenomena in the Macroscopic World*, IOP 2005.
21. O. C. Zienkiewicz, R. L. Taylor, *The Finite Element Method, Volume 2, Solid Mechanics*, Butterworth-Heinmann 2000.
22. E. Idczak, T. Strek, *Minimization of Poisson's ratio in anti-tetra-chiral two-phase structure*, IOP Conf. Ser.: Mater. Sci. Eng., **248** (2017) 012006.
23. T. Stręk, H. Jopek, E. Idczak, K. W. Wojciechowski, *Computational Modelling of Structures with Non-Intuitive Behaviour*, Materials, **10** (2017) 1386.
24. M. Nienartowicz, T. Stręk, *Modeling and FEM analysis of dynamic properties of thermally optimal composite materials*, 11th World Congress on Computational Mechanics, WCCM 2014, 5th European Conference on Computational Mechanics, ECCM 2014 and 6th European Conference on Computational Fluid Dynamics, ECFD 2014.

The Influence of the Lubrication on the Vibroacoustic Signal Generated by Rolling Bearings

Bartosz JAKUBEK

*Poznan University of Technology, Faculty of Mechanical Engineering and Management,
3 Piotrowo St, 60-965 Poznan; bartosz.jakubek@put.poznan.pl*

Roman BARCZEWSKI

*Poznan University of Technology, Faculty of Mechanical Engineering and Management,
3 Piotrowo St, 60-965 Poznan; roman.barczewski@put.poznan.pl*

Michał JAKUBOWICZ

*Poznan University of Technology, Faculty of Mechanical Engineering and Management,
3 Piotrowo St, 60-965 Poznan; michal.jakubowicz@put.poznan.pl*

Abstract

Long-life and failure-free operation of rolling bearings depends on the proper lubrication. Additionally lubrication reduces vibration and noise generated by the operating bearing. However, from the point of view of the post-production diagnostics, lubrication can lead to undesirable masking of damage and manufacturing defects. This article presents the comparison of parameters of vibroacoustic signals generated by tapered roller bearings under different lubrication conditions. The influence of the lubricant on the form of vibroacoustic signals in both amplitude and frequency terms was determined. The premises on the choice of the lubricant for the post-production diagnostics of rolling bearings have also been specified.

Keywords: tapered roller bearings, lubrication, post-production diagnostics

1. Introduction

The purpose of the rolling bearings' lubrication is to separate the metal rolling elements and the races by a thin lubricant layer. This provides among others the reduction of friction in the rolling bearing, as well as an improvement of tribological properties and increase of operational reliability [1, 2]. Moreover, proper lubrication of rolling bearings provides: protection against corrosion and contamination, better heat dissipation, as well as noise reduction. The choice of the lubricant depends on: the type of rolling bearing, the material of the cage (metal or plastic) and operating parameters such as: nominal operating temperature, rotation speed range, load and environmental conditions [3-5].

The fulfilment of all mentioned earlier purposes of the lubrication is expected from the point of view of the operation [6]. On the other hand, the presence of a lubricant can significantly influence the form of vibroacoustic (VA) signals generated by the rolling bearing, both in qualitative and quantitative terms. Most of the diagnostic methods are based on measurements and analyses of vibrations and noise [7, 8]. Hence the type of the used lubricant is relevant. This influence should be taken into consideration during the post-production diagnostics of the rolling bearings. The ISO standard 15242 *Rolling bearings – Measuring methods for vibration* orders to:

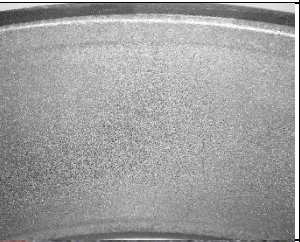
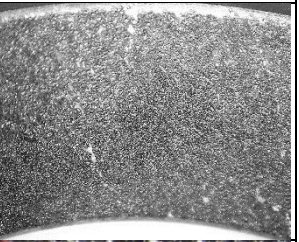
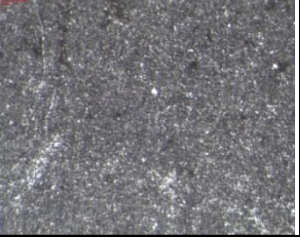
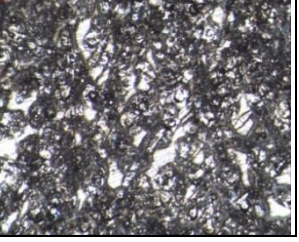
- test pre-lubricated bearings in the so-called delivery condition
- lubricate unlubricated bearings before testing with oil of viscosity from 10 mm²/s to 100 mm²/s (adequate for the type and the size of a bearing).

It is noted that some of anti-corrosive materials meeting lubrication criteria can also be used while measurements [9].

2. Experiment setup

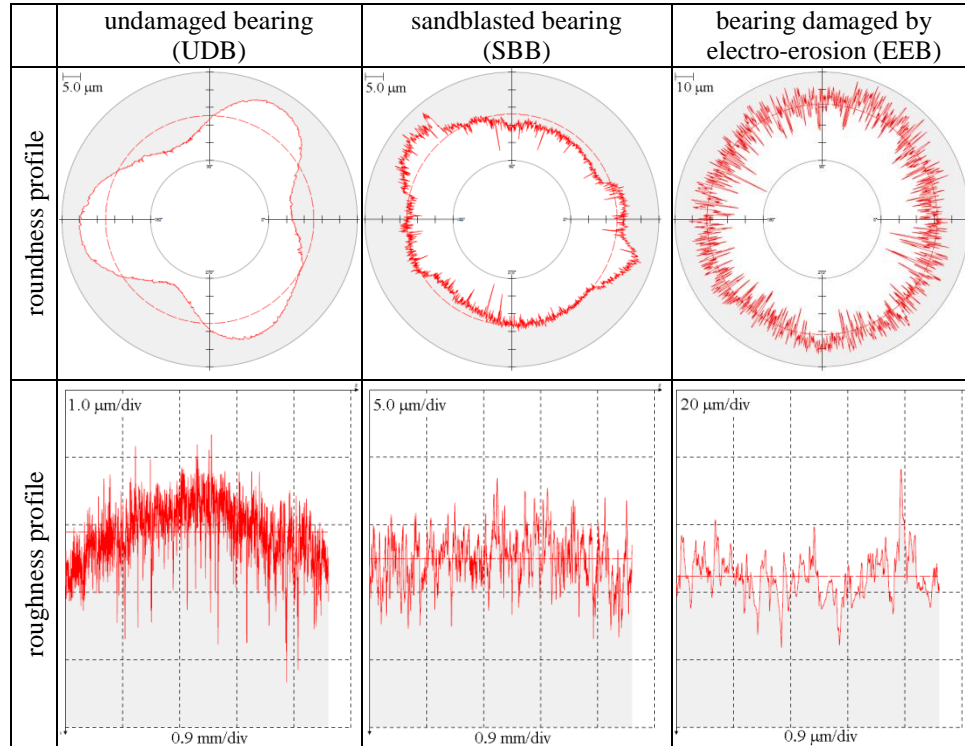
The aim of the research was to compare quantitative (measures) and qualitative (characteristics) changes in the vibration signals generated by rolling bearings as a result application of various lubricants. The tests were carried out using three CBK 171 tapered roller bearings with varying damage intensity. Among them there were one undamaged bearing (UDB), one sandblasted bearing (SBB) and one bearing damaged by electroerosion (EEB). Imperfections was introduced on the entire surface of the outer races. It should be noted that the remaining bearing parts (rollers, inner races) were free from defects and damage. Pictures of outer races of testing bearings (views and magnifications) are presented in Table 1.

Table 1. Outer races of the set of testing bearings

	undamaged bearing (UDB)	sandblasted bearing (SBB)	bearing damaged by electroerosion (EEB)
view			
magnification			

Before testing, the outer races (UDB, SSB, EEB) were parameterized on a coordinate measuring machine. The roundness and the roughness deviations (Table 2) were measured with specialized instrument Hommel-Etamic roundscan 535. The machine was equipped with Turbo Form software for the analysis of shape errors by the contact method. In this case, the measurements of the roundness deviation were carried out by a non-floating method.

Table 2. The results of geometric measurements of outer races of testing bearings (pay attention for different scales)



The acquisition of the vibroacoustic signals was carried out on a test stand (sampling frequency was equal to 96 kHz). Experiments have been performed with specified operating parameters such as: radial load equal to 15 N, axial load equal to 55 N and rotation speed of inner ring equal to 1450 rpm. The measurements of rotation speed and analysis of vibrations and noise generated by the bearings were repeated for different types of lubricants. Table 3 contains the description of the used lubricants.

The vibration accelerations and the noise were linearly recorded (up to 50 kHz). Signal sequences (180-second long) have been acquired. The ICP ® M352A60 (PCB) accelerometer was used for vibrations measurements. The noise measurements were made by the polarized free-field microphone G.R.A.S. 40BF compatible with the low noise preamplifier Brüel & Kjaer NEXUS type 2691. The acquisition module VibDAQ 4+ was used for the analogue-digital conversion of VA and tachometer signals. Data acquisition ran synchronously on 4 channels. Digital signal processing was performed using a dedicated software elaborated in DASyLab® Data Acquisition System Laboratory.

The bearings were carefully prepared before testing. They were cleaned (duration 3 min) in an ultrasonic cleaner filled with kerosene and then rinsed in petroleum ether. Before each test the cleaning procedure was repeated twice. Oils (1/8 ml volume) were dosed precisely with a syringe to the bearing previously mounted on the stand whereas greases (approx. 1/3 g) were applied before mounting the bearing on the stand.

Table 3. Types and codes of the tested lubricants

Lubricant	Code
silicon oil	A
hydraulic oil	B
gear oil	C
universal grease, class NLGI: 2	D
long-lasting grease, class NLGI: 2, KP2 K-30	E
high pressure grease with MoS ₂ , class NLGI: 2, KP2 K-30	F
copper mounting paste	G

3. Results

The influence of the lubricant on the change of the VA signals was considered both in quantitative and qualitative terms.

The quantitative analysis was performed basing on the observation of instantaneous peak values of vibration acceleration a_{peak} determined from 84 ms long signal sequences. This measure, for sampling frequency $f_s = 96$ kHz, allows the observation of instantaneous changes in the VA signal (with minimal duration approx. 10 μ s). It is worth mentioning that the RMS value of the signal, which is widely used in technical diagnostics, as an integration operator (it has averaging properties) is much less suitable to detection of the instantaneous changes of the VA signals. The vibrations were measured on the bearing housing in the radial direction.

The qualitative analysis (time-frequency analysis) was performed basing on both for the bearing housing vibrations and noise generated by operating bearing. The noise has been recorded at a distance of 100 mm from the bearing (along axis of rotation).

The research in quantitative term was conducted using three previously described testing bearings (UDB, SSB, EEB). Figure 1 shows the changes in the instantaneous a_{peak} values resulting from the use of different lubricants. The graphs illustrate changes that occurred in the first 180 seconds after the beginning of the test.

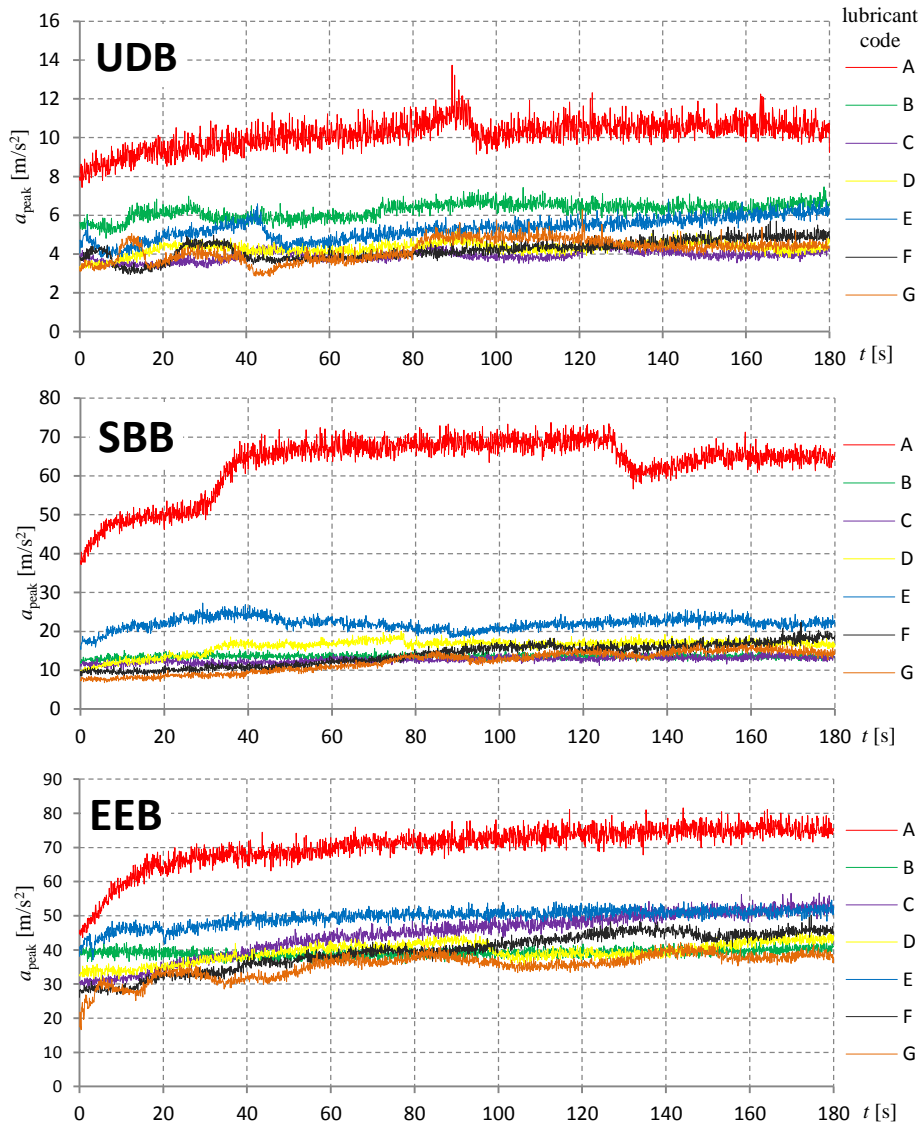


Figure 1. Instantaneous peak values of vibration acceleration (the value axis has been auto-scaled in order to better visualize the changes of a_{peak})

For all bearings, the highest instantaneous a_{peak} values through all the testing time (180 s) have been observed while silicone oil (A) was used. This means that lubricants with low viscosity slightly mask the appearance of defects and damage of bearings in the vibration signal.

Instantaneous a_{peak} values were noticeably lower in the case of the other lubricants. Therefore the masking of defects and race damage took place. Among the other lubricants the lowest instantaneous a_{peak} values were noted while grease (G) was used regardless of the intensity of the race damage. It is worth mentioning that when the intensity of defects and damage is small similar masking occurs while lubricating with oil (C).

There were 4 levels of defect masking introduced: low, moderate, significant and superior. They allow for an approximate classification of lubricants. A categorisation of the tested lubricants in terms of the masking levels is provided in Table 4.

Table 4. The level of masking of defects and damage in vibration signal of rolling bearings for tested lubricant.

level of defect masking	undamaged bearing (UDB)	sandblasted bearing (SBB)	bearing damaged by electro-erosion (EEB)
low	A	A	A
moderate	B	E	E
significant	D, E, F	B, D, F	B, C, D, F
superior	C,G	C,G	G

Table 5 shows the expanded parameterization of instantaneous a_{peak} values in the first 180 s from the beginning of the test. The highest peak value (\hat{a}_{peak}), the lowest peak value (\check{a}_{peak}) and the mean peak value (\bar{a}_{peak}) were determined for the considered period of time. In addition, the standard deviation (σ) and standard deviation normalized to mean peak value (σ/\bar{a}_{peak}) were determined.

Table 5. The expanded parametrization of the instantaneous a_{peak} values of vibration accelerations in the first 180 s from the beginning of the test

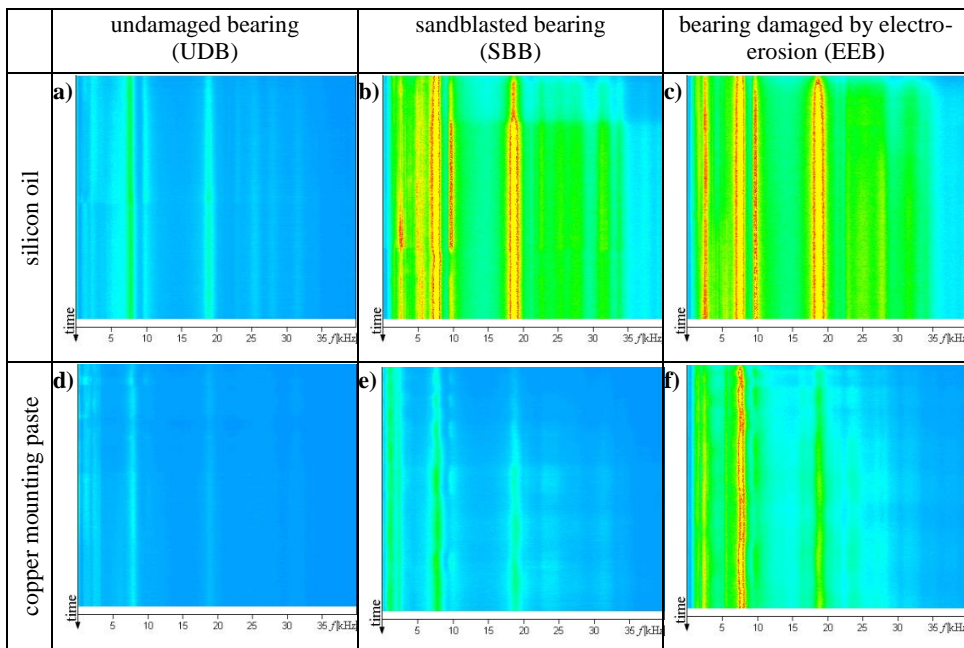
lubricant type	undamaged bearing (UDB)					sandblasted bearing (SBB)					bearing damaged by electroerosion (EEB)				
	\check{a}_{peak}	\hat{a}_{peak}	\bar{a}_{peak}	σ	$\frac{\sigma}{\bar{a}_{peak}}$	\check{a}_{peak}	\hat{a}_{peak}	\bar{a}_{peak}	σ	$\frac{\sigma}{\bar{a}_{peak}}$	\check{a}_{peak}	\hat{a}_{peak}	\bar{a}_{peak}	σ	$\frac{\sigma}{\bar{a}_{peak}}$
A	7.43	13.74	10.18	0.75	0.07	37.21	73.75	63.09	7.44	0.12	43.60	81.55	70.46	6.08	0.09
B	4.81	7.47	6.25	0.41	0.07	11.30	15.60	13.52	0.56	0.04	35.82	42.99	39.18	1.15	0.03
C	3.22	4.69	3.91	0.27	0.07	10.07	15.20	12.69	0.79	0.06	28.55	56.69	44.64	6.47	0.14
E	3.18	5.33	4.30	0.30	0.07	9.52	20.02	16.17	1.86	0.11	30.65	45.77	39.36	2.83	0.07
F	3.68	6.84	5.31	0.57	0.11	15.34	27.25	21.95	1.63	0.07	37.07	54.59	49.55	2.53	0.05
G	2.95	5.70	4.24	0.49	0.12	8.51	22.33	13.90	2.89	0.21	26.08	50.15	39.63	5.40	0.14
H	2.85	6.29	4.23	0.55	0.13	6.74	16.96	12.19	2.62	0.21	16.66	42.22	35.34	3.62	0.10

The mean peak value \bar{a}_{peak} (averaged in 180 s) was proposed to the assessment of the level of defect masking in the VA signal. The higher the value of this parameter, the less

the defect is masked. Therefore, for the purpose of post-production diagnostics of the rolling bearings, it is justified to use lubricants for which \bar{a}_{peak} reaches the highest values (the lowest level of defect masking). Among the considered lubricants this criterion is best met by oil (A) regardless of the intensity of the race damage.

On the other hand, basing on the standard deviation normalized to the mean peak value ($\sigma/\bar{a}_{\text{peak}}$), the amplitude stationarity of the whole 180-second testing process can be determined. In order to obtain low measurement uncertainty, the lowest possible value of this parameter is desired. From this point of view, the oil (B) best meets this criterion, while oil (A) does the same only for undamaged bearing (UDB).

Table 6. Spectrograms of vibration accelerations of the bearing housing for lubricants: silicon oil (A) and copper mounting paste (G)



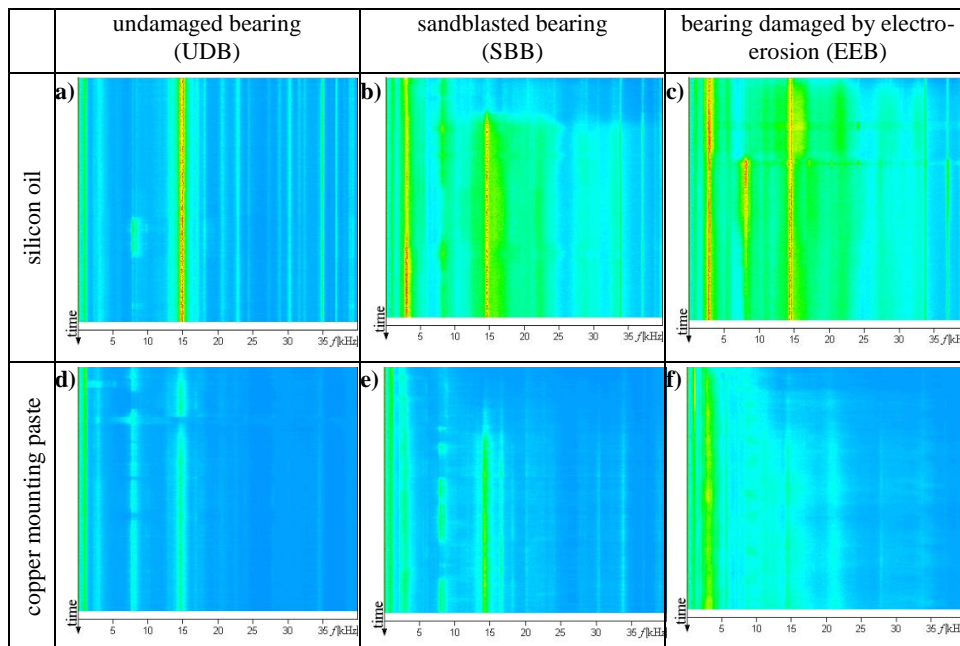
The spectrograms of vibration accelerations of the bearing housing (Table 6) and of acoustic pressure (Table 7) allow us to compare the influence of the used lubricants on the VA signal in the quality term. The comparison concerns the use of oil (A) (the least masking) and grease (G) (the most masking). The figures in Table 6 and Table 7 (short-time spectra) illustrate changes occurring through all the testing time (180 s).

The signal components associated with the eigenfrequencies of the bearing-housing system (about 7.5 kHz and about 19 kHz) are clearly visible on all the vibration spectrograms (Table 6). According to ISO 15242, it is recommended to measure vibration velocity in the frequency band from 50 Hz to 10 kHz [9]. Spectrogram analysis demonstrates that in case of the used test stand it is possible and justified to perform measurements and analyses of vibration accelerations in the extended frequency band up

to 50 kHz. The spectrum above 10 kHz apart from resonance vibration of the stand contain components related to defects and damage of the bearing. Therefore limiting the measurement bandwidth in accordance with ISO 15242 only to 10 kHz may deprive us of essential diagnostic information. It can be observed that some of the high frequency components of the signal appear with a delay to the beginning of the test. This is clearly visible for damaged bearings (see Table 7, Figures b, c, e and f). It mainly relates to the distribution of the lubricant in the bearing. In practical approach, the use of the band-stop filtering in resonance bands should yet be considered.

The vibration and noise spectrograms are similar in quality term. Theoretically the acoustic signal compared to the vibration accelerations is more sensitive to the environment noise. However the tests carried out prove that it is worth taking into account the results of measurements and analysis of noise in the post-production diagnostics of rolling bearings.

Table 7. Spectrograms of acoustic pressure measured in the distance of 100 mm from the bearing for lubricants: silicon oil (A) and copper mounting paste (G)



4. Summary

The carried out tests allowed the formulation of the following conclusions. In order to obtain reliable results it is necessary to properly prepare the bearings to the tests (especially cleaning them).

The \bar{a}_{peak} parameter can be used to assess the level of defect masking in the VA signal by the used lubricant. The $\sigma/\bar{a}_{\text{peak}}$ parameter can be used to determine the stationarity of the testing process.

Among the tested lubricants, low viscosity oil (A) had the best features for post-production bearing testing. Due to the significant level of defect masking greases should not be used for post-production diagnostic purposes (compare table 6 pictures a and e). This confirms the recommendations of ISO 15242.

The noise and vibration spectrograms clearly show signal changes in quality term. They also allow the specification of the time from the beginning of the test, in which VA signals can be treated as quasi-stationary.

Spectrograms have shown the purposefulness of taking into account components in the higher frequency band (over 10 kHz). Extraction of resonance components should be considered.

The results of the carried out tests have shown that the improper type of lubricant used for post-production diagnostics can lead to the masking of manufacturing defects. As a consequence, this may reduce the reliability and the accuracy of the classification in categories of good / bad and significantly reduce the possibility of defect detection.

Acknowledgment

The results presented are results of the research that was partially funded with grants 02/21/DSMK/3482 and 02/21/DSPB/3494 for education allocated by the Ministry of Science and Higher Education of the Republic of Poland.

References

1. G. Mullett, *Grease lubrication of rolling bearings*, Tribology, **6** (1973) 21 – 28.
2. FAG Kugelfischer Georg Schäfer AG, *Rolling Bearing Lubrication*, Publ. No. WL 81 115/4 EA.
3. A. Mizerski, *Smarowanie łożysk w przemyśle – nowe wyzwania*, Industrial Monitor, **10** (2013) 64 – 66.
4. M. Fidali, *Smarowanie łożysk tocznych*, Industrial Monitor, **21** (2016) 40 – 44.
5. D. Stöckl, K. Grissenberger, *Smarowanie łożysk walcowych*, Industrial Monitor, **22** (2016) 38 – 40.
6. M. R. Balan, A. Tufescu, S. S. Cretu, *A case study on relation between roughness, lubrication and fatigue life of rolling bearings*, Materials Science and Engineering, **147** (2016) 1 – 12.
7. R. Randall, J. Antoni, *Rolling element bearing diagnostics – A tutorial*, Mechanical Systems and Signal Processing, **25** (2010) 485 – 520.
8. R. Randall, *Vibration-based Condition Monitoring: Industrial, Aerospace and Automotive Applications*, Wiley, New Delhi, 2011, 67 – 71.
9. ISO 15242-1(2015) Rolling bearings – Measuring methods for vibration – Part 1: Fundamentals.

Evaluation of a Simple Method of Identification of Dynamic Parameters of a Single-Degree-of-Freedom System

Maciej TABASZEWSKI

*Institute of Applied Mechanics, Poznan University of Technology, 3 Piotrowo Street,
60-965 Poznań, maciej.tabaszewski@put.poznan.pl*

Małgorzata WOJSZNIS

*Institute of Applied Mechanics, Poznan University of Technology, 3 Piotrowo Street,
60-965 Poznań, malgorzata.wojsznis@put.poznan.pl*

Abstract

The paper presents a simple method of identification of dynamic parameters of single-degree-of-freedom systems based on an impulse test. Numerical simulations consisting in generating a model impulse excitation and the response of a model system with specified dynamic parameters to this excitation have been carried out to present the applicability range of the method. The influence on parameter estimation errors at various set values of these parameters and procedure parameters has been investigated.

Keywords: impulse test, identification of dynamic parameters, single-degree-of-freedom system

1. Introduction

To identify selected or all dynamic parameters, such as damping, stiffness and mass of a vibrating linear single-degree-of-freedom system it is possible to use many methods, from the simplest ones based on free vibrations and investigation of the influence of the test mass to harmonic or impulse tests [1, 2].

In the paper a method based on approximation of an experimentally determined frequency response function (FRF) is described. This function can be described for a single-degree-of-freedom systems as [3]:

$$H(j\omega) = \frac{X(j\omega)}{F(j\omega)} = \frac{\frac{1}{m}}{-\omega^2 + j\omega \frac{c}{m} + \frac{k}{m}} = \frac{\frac{1}{m}}{-\omega^2 + 2j\omega h + \omega_o^2}, \quad (1)$$

where: $H(j\omega)$ is the dynamic compliance, m – mass, k – stiffness coefficient, c – damping coefficient, $X(j\omega)$ is the system response in frequency domain, $F(j\omega)$ is the system excitation in frequency domain, j – imaginary unit, $\omega = 2\pi f$, $2h = c/m$, and ω_o is the frequency of free undamped vibrations.

The used identification methods were based on empirical determination of characteristics H_1 or H_2 according to the following definition:

$$H(j\omega) = H_1(j\omega) = \frac{G_{FX}(j\omega)}{G_{FF}(j\omega)}, \quad (2)$$

$$H(j\omega) = H_2(j\omega) = \frac{G_{XX}(j\omega)}{G_{XF}(j\omega)}, \quad (3)$$

where: $G_{FX}(j\omega)$ – cross power spectral density of the excitation and response signals, $G_{FF}(j\omega)$ – auto power spectral density of the excitation signal, $G_{XF}(j\omega)$ – cross power spectral density of the response and excitation signals, and $G_{XX}(j\omega)$ – auto power spectral density of the response signal. In case of absence of any disturbances both characteristics give the same results. In the event, however, where there are disturbances in the response signal, better results are obtained with characteristic H_1 , and in case of disturbances in the excitation signal better results gives characteristic H_2 .

The auto spectral density of signal x is estimated as [2]:

$$G_{xx}(\omega_k) = \frac{2\Delta t}{N} |X(\omega_k)|^2, \quad (4)$$

where: $X(\omega)$ – complex spectrum of the signal, Δt – sampling period, N – number of samples, k – consecutive number of a spectral line, and $|X(\omega_k)|^2 = X_{\text{Re}}^2(\omega_k) + X_{\text{Im}}^2(\omega_k)$.

By analogy, cross power spectral density of signals x and y may be expressed as:

$$G_{xy}(\omega_k) = \frac{2\Delta t}{N} [X^*(\omega_k)Y(\omega_k)]. \quad (5)$$

where: $X^*(\omega_k)$ - complex conjugate of a complex number.

Determination of a spectrum consists in computation of a discrete Fourier transform (most often with use of FFT algorithm):

$$X(k\Delta f) = \frac{1}{N} \sum_{k=0}^{N-1} x(n\Delta t) e^{-j2\pi k n / N}, \quad (6)$$

where: $x(n\Delta t)$ – signal sample, n – consecutive number of the signal sample.

The essential part of the algorithm in use is approximation of the experimentally determined characteristic H_1 or H_2 by means of the least square method. One can easily see that formula (1), taking the absolute value of the characteristic into account, can be written as:

$$|H| = \frac{1}{m} |A|, \quad (7)$$

where: $A = \frac{\omega_0^2 - \omega^2 - 2j\omega h}{(\omega_0^2 - \omega^2)^2 + 4\omega^2 h^2}$, $\text{Im}(A) = -2h\omega / B$, $\text{Re}(A) = (\omega_0^2 - \omega^2) / B$

and $B = (\omega_0^2 - \omega^2)^2 + 4h^2\omega^2$, $A = j \cdot \text{Im}(A) + \text{Re}(A)$, $|A| = \sqrt{\text{Im}^2(A) + \text{Re}^2(A)}$

Using the least square method one can determine the reciprocal of mass $\varphi = 1/m$ fitting model (7) to the experimentally obtained characteristic:

$$\varphi = (\mathbf{A}^T \mathbf{A})^{-1} \mathbf{A}^T \mathbf{H}, \quad (8)$$

where:

$$\mathbf{H} = \begin{bmatrix} |H_1| \\ |H_2| \\ \dots \\ |H_{N/2}| \end{bmatrix} \quad \mathbf{A} = \begin{bmatrix} |A_1| \\ |A_2| \\ \dots \\ |A_{N/2}| \end{bmatrix}$$

H_k – vector of discrete values of characteristic H obtained experimentally, and $A_k = A(\omega_k)$. By means of the above we can determine the unknown parameter of mass. In the first step, however, vector \mathbf{A} should be known. Elements of this vector may only be determined when parameters h and ω_0 of the investigated system are known. We will further assume that the damping is not so high.

Using the method of half power and the assumption of system linearity (the assumption of symmetry of the characteristic around the eigenfrequency) one can estimate coefficient h [3]:

$$h = \frac{\Delta\omega}{2} = \frac{\omega_2 - \omega_1}{2} \quad (9)$$

where: ω_1 and ω_2 are determined in such a way that the following condition is fulfilled:

$$|H(j\omega_1)| = |H(j\omega_2)| = \frac{|H(j\omega_0)|}{\sqrt{2}} \quad (10)$$

As the obtained characteristic H is discrete, it is worthwhile using here interpolation to determine ω_1 and ω_2 more accurately.

In accepting some error by assumption of small damping one can determine ω_0 by finding the frequency, which corresponds to the local minimum of the imaginary part of the FRF characteristic.

The use of the least square method (8) enables to fit the model function $|H|$ and to identify the mass parameter. This in turn, with the assumption of ω_0 , enables to estimate stiffness parameter k and c .

2. Testing of procedures

It should be pointed out that in practice the errors of parameter estimation may depend on many factors. The errors will stem from the assumption of small damping in the system, the approximation of power spectral densities, the matching of the model characteristic, and from parameters of signal sampling.

To estimate the applicability range of the discussed simple method of parameter estimation some numerical simulations were performed. The simulations consisted in generation of a response of a system with defined parameters to the excitation in the form of an impulse, which duration was equal to the simulated sampling period and which had an assumed amplitude. The response signal in frequency domain was determined from equation (1). In the next step the response signal in time domain was obtained by means

of the inverse Fourier transform. The generated signals created an input to the previously described procedure. Such an approach made it possible to simulate to a certain degree a situation of a real measurement. Obviously in a real experiment one should expect much more sources of errors, but identification of those which stem from the procedure itself seems valuable.

As simulation parameters were used both dynamic parameters of the system: c , k , m and sampling frequency f_p and the number of samples used for the analysis N . Both the latter ones were expressed by resolution:

$$\Delta f = \frac{f_p}{N} \quad (11)$$

whereby the sampling frequency ensured the actual analysis band, encompassing with a large excess the natural frequency of the simulated system.

Examples of the excitation and system response are shown in figure (1).

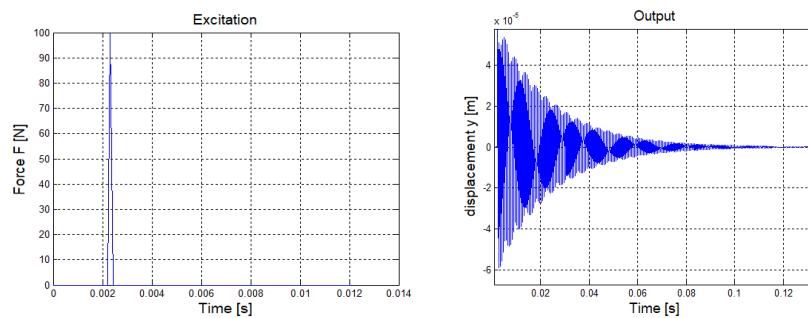


Figure 1. Example of the simulated excitation and the response of the modelled system

A very important problem in the algorithm is the quality of fitting the model characteristic (1) to the obtained simulated $|H|$. Figure 2 shows an example of fitting (solid line) to a numerically determined characteristic (points). Figure 3 shows errors of identification of the mass parameter using the presented procedure at constant assumed stiffness $k = 1\text{MN/m}$ and constant resolution $df = 0.255\text{Hz}$ (11).

As it can be seen from the presented sample analyses (figure 3), with the increase in the mass the values of errors increase unacceptably. For small masses, corresponding to frequencies f_0 higher than 700 Hz (for the assumed parameters) the errors are smaller than 5%, for lower frequencies, however, the estimation accuracy depends strongly on the value of the damping coefficient – the higher the better. In relation to the assumption of small damping this seems to be surprising. This, however, results from the fact, that at the defined resolution of the spectral analysis the determination of damping by means of the full width at half maximum (fwhm) method (formulae (9) and (10)) will be relatively more accurate for higher values of resonance breadth than for the lower ones. High inaccuracy of estimation of h influences the identification of the values of remaining parameters significantly. Moreover, it should be pointed out that in the presented simulations the requisite of a small damping value is fulfilled anyway even for the highest values of c ,

because the dimensionless damping coefficient does not exceed here the value of 0.01. Figure 3 indicates also that generally with the increase in the damping the approximation error of characteristic $|H|$ measured with error MSE decreases. For very small damping the characteristic is very smooth, which causes some problems at fitting. It should be noted, that for very small damping determination of the maximum value of the characteristic may be very difficult and the results should be treated as approximate.

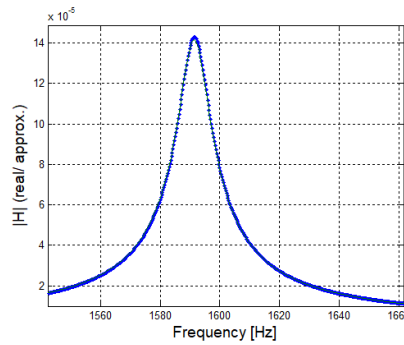


Figure 2. Example of an obtained characteristic $|H|$ (points) and its approximation (solid line)

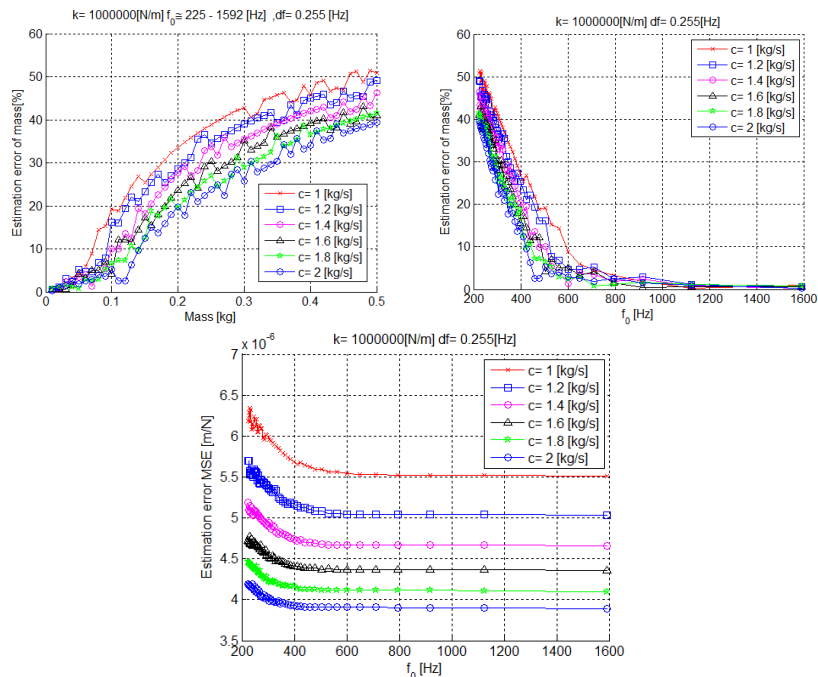


Figure 3. Sample result of simulation for different masses of the system and estimation of mass for resolution of 0.255Hz

Next figure shows the improvement of the accuracy of the estimation of mass with the increase in resolution adjusted by means of the number of samples. Unfortunately in practice increasing the number of samples may cause some problems related to the analysis of the response signal, which may disappear in a relatively short period of time in comparison to the analysis time. This will cause, that the noise recorded after disappearance of vibrations will be analyzed as well.

Examples of another simulations are shown in figure 5, where the estimation error of the stiffness parameter and the MSE error of the fitting of model characteristic $|H|$ to the simulated data are shown. As it can be seen in the first two graphs the estimation error of stiffness is, for the assumed constant mass, acceptable and depends on the assumed stiffness of the model. Whereas with the increase in stiffness, or the value of f_0 , the MSE error decreases significantly. Hence, at the identification of mass of the system the MSE error may provide an indication as to the estimation accuracy of parameter m , but in case of identification of k such an indication does not exist. This stems from the fact, that the stiffness parameter is not identified by means of equation (8).

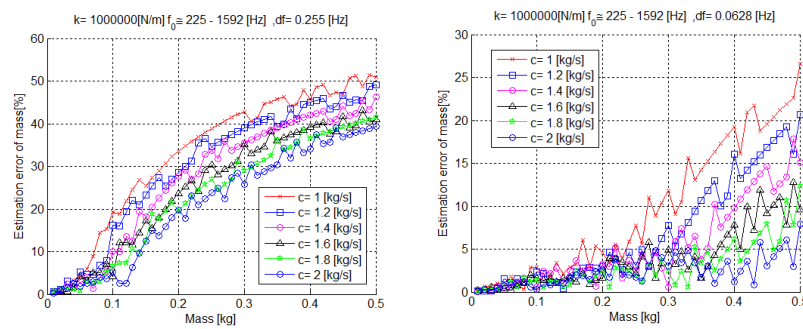


Figure 4. Sample simulation results for different masses of the system and estimation of mass for resolutions of 0.255Hz and 0.0628Hz

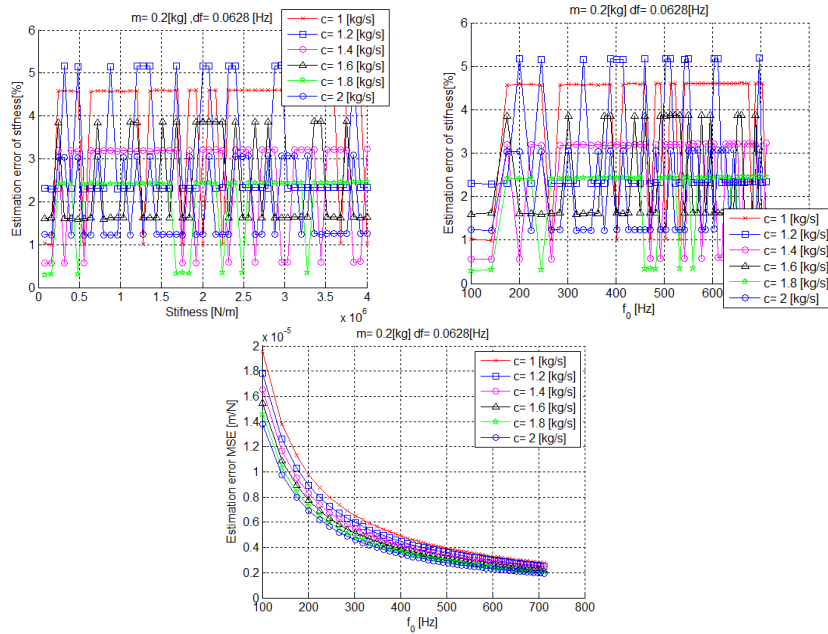


Figure 5. Sample simulation results for different stiffness and estimation of stiffness

Figure 6 shows a simulation concerning a change in system damping at a specified stiffness and mass. The damping properties are presented in categories of coefficient c and dimensionless damping coefficient ξ . As it can be seen, too small values of parameter c make the proper identification of this quantity difficult. For the values of the dimensionless damping coefficient lower than 0.005 (at the specified resolution) the errors of estimation can be higher than 5%.

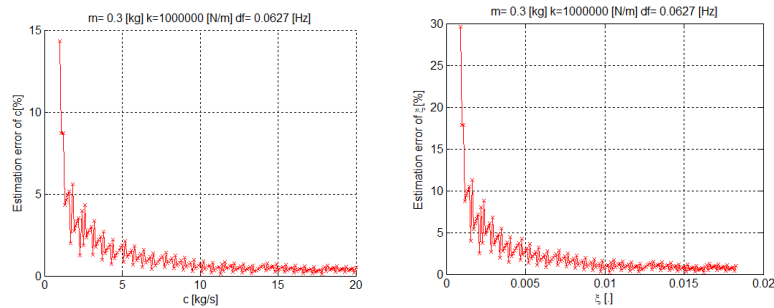


Figure 6. Sample results of simulation for different damping of the system and estimation of damping

3. Conclusions

The presented simple method of identification of dynamic parameters gives satisfactory results only within a certain range of these parameters. What is crucial here is the damping in the system. In the in simulations investigated range of values the method performs better for higher values of damping rather than for the lower ones, which is caused by errors in approximation of very narrow characteristics $a-f$ and by too big errors in determination of full width at half maximum of the resonance in such cases. The situation can be improved by increasing the resolution of the analysis, but in practice such a possibility is limited. The correctness of identification of parameters cannot be evaluated directly by the analysis of quality of fitting of the model to characteristic $|H|$. It should also be noted that in the adopted method the errors in determination of parameters are of a different nature for different physical quantities. Assuming the remaining parameters to be constant – for the mass the error increases with its increase, i.e. decreases with the increase in f_0 . For the stiffness it does not depend monotonically neither from its value nor from f_0 . For the damping it decreases with its increase (for the investigated range of parameters).

Generally, as a result of the performed simulations and analyses it can be said that for damping values $\xi > 0,01$, free vibration frequencies $f_0 > 600\text{Hz}$ and for resolution $\Delta f \leq 0.255\text{ Hz}$ the obtained estimated values of dynamic parameters do not differ from the real ones by more than 10%. In case of actual measurements one can expect higher error values, which is due to measurement uncertainties of the measured quantities, which were not taken into account in the presented simulations.

Acknowledgments

The presented research results, were funded with grants for education allocated by the Ministry of Science and Higher Education in Poland 02/21/DSPB/3494.

References

1. J. Giergiel, T. Uhl, *Identyfikacja układów mechanicznych*, PWN, Warszawa 1990,.
2. T. Uhl, *Komputerowo wspomagana identyfikacja modeli konstrukcji mechanicznych*, WNT, Warszawa 1997.
3. S. Gade, H. Herlusfen, *The use of Impulse Response Function for Modal Parameter Estimation*, Technical Review, No. 2, Bruel & Kjeear A/S 1994.

A Small-Size Stand for Vibroacoustic and Durability Testing of Rolling Bearings

Mateusz WRÓBEL

*Poznan University of Technology, Faculty of Mechanical Engineering and Management,
3 Piotrowo St, 60-965 Poznan; mateusz.k.wrobel@doctorate.put.poznan.pl*

Roman BARCZEWSKI

*Poznan University of Technology, Faculty of Mechanical Engineering and Management,
3 Piotrowo St, 60-965 Poznan; laboratoria@tlen.pl*

Abstract

A small-size stand for vibroacoustic and durability testing of rolling bearings is presented in this paper. Main purposes and motivations for building this stand were not only to assist research and development works but also to familiarize students with techniques and methods of rolling bearings diagnosing as well as to improve their skills of assessment of rolling bearings technical condition. The project assumptions of the stand, mechanical construction and architecture of data acquisition and analysis system (hardware and software) are described in this paper. Finally there are conclusions about stand's capabilities included.

Keywords: vibroacoustics, rolling bearings, durability tests, testing stand

1. Introduction

In the research and development works in the field of rolling bearings technical diagnostics there is a need of disposing of signals and measurement data. The data should preferably comply the entire cycle of rolling bearings life – from a brand-new state to the moment of its full technical degradation. This data may be obtained from machines during their regular work in industrial conditions. It is common that such data are not complete enough to form full symptom life curves of rolling bearings'. The full informative data may be obtained from dedicated for long-term durability testing stands. This devices are usually equipped with a hydraulic load control system. Such a solution provides a possibility to load the testing bearing with forces far above its dynamic load capacity. Stands of this type are usually big and they are very expensive [1].

Considering above, it was justified to design and build a small-size, low-cost stand for vibroacoustic and durability testing of rolling bearings. The elaboration of the stand was also important because many methods of rolling bearings diagnosing use vibroacoustic signals to assess technical condition of rolling bearings. These methods include: wideband root-mean-square (RMS) vibration measurement [2], shock pulse method (SPM) [3], kurtosis determination, crest factor measurement [4], analysis of vibration signal envelope [5], spectral analysis [6] and the use of Teager-Kaiser energy operator [7]. The stand is mainly dedicated to didactical purposes but it also should enable R&D works targeting development of new methods and techniques of the rolling bearings diagnosing. The stand's hardware (including mechanical part) and software should support laboratory

classes where students improve their skills in assessment of the rolling bearings technical condition [8].

The long-term testing of rolling bearings on this stand includes all phases of rolling bearings technical degradation. The testing shall also guarantee simultaneous registration of vibroacoustic signals, thermal and work parameters. In this way it is possible to create data libraries which may be used to perform different multi-thread analyses on workstations which are not directly connected with the stand. The collected data may be used for determination of rolling bearings symptom life curves and then for estimation of alert thresholds for specific bearings types [9].

2. Research object and design assumptions

The stand was designed for self-aligning UC205 rolling bearings or other bearings with similar dimensions. Basic parameters of UC205 rolling bearing are shown in Table 1. This specific type of rolling bearings has been chosen as the research object because of possibility of using a typical tension housing. Therefore the bearing can set its position in the housing relative to shaft and housing.

Table 1. Basic parameters of rolling bearing UC205

Inner diameter	25 mm
Outer diameter	52 mm
Static load capacity	7880 N
Dynamic load capacity	14000 N
Maximum operating temperature	110°C

The following parameters has been taken into account at the design stage:

- compact construction – small size compared to professional stands offered on the market,
- low power consumption; power supply 230 V (single-phase),
- automatic emergency stop in case of:
 - exceeding the vibration threshold,
 - exceeding the temperature threshold,
 - unexpected decrease of motor RPM as an effect of drive unit overload,
- possibility of fluent radial loading of tested bearing in the range 0 – 2000 N.

3. Mechanical part of stand

Mechanical part of the stand is shown in Figure 1. The drive unit of the stand is a single-phase asynchronous 0.75 kW electric motor. The tested bearing is mounted on a separate shaft. This shaft is supported by two rolling bearings with significantly higher dynamic load capacity compared to the tested bearing. The electric motor drives the shaft with the tested rolling bearing by a belt transmission with 2:1 gear ratio. Therefore degradation of the tested bearing is much more intensive and frequent replacement of support bearings

can be avoided. The loading system consists of a set of parallel springs. It loads the tested bearing with maximum force of 2400 N. The load value is calculated on the base of springs' deflection which optionally can be measured manually using e.g. a calliper or by an optical sensor. The mechanical part of the stand is mounted in a steel frame with dimensions of $0.4 \times 0.5 \times 0.4$ m. It should be mentioned that the drive unit is vibroisolated using rubber elements between the steel frame and heavy concrete base of the electric motor.

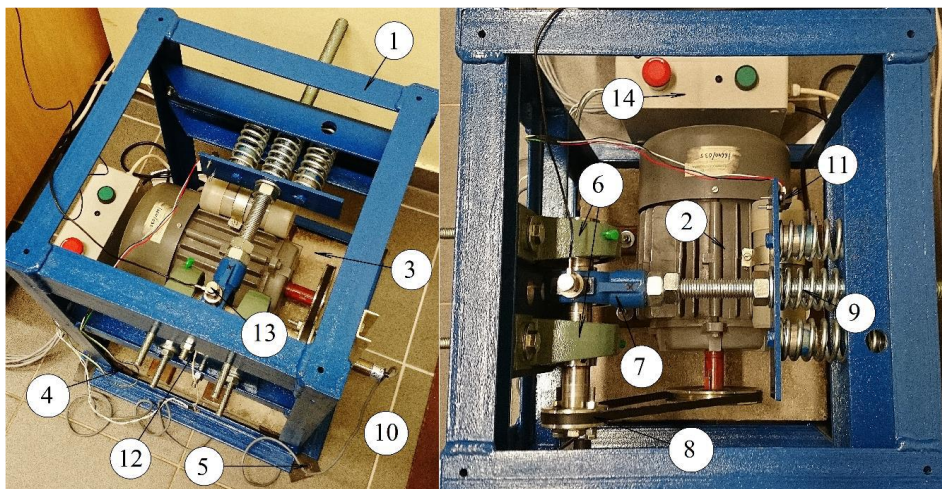


Figure 1. Mechanical part of the rolling bearings testing stand (1 – steel frame, 2 – electric motor, 3 – motor base, 4 – vibroisolation, 5 – rubber separation elements, 6 – support bearings, 7 – tested bearing in tension housing, 8 – belt transmission, 9 – springs loading system, 10 – tachometer (RPM measurement), 11 – optical sensor (springs deflection measurement), 12 – temperature sensor (temperature measurement), 13 – vibration transducer (piezoelectric accelerometer), 14 – signal acquisition and motor control device (the SAMC device))

4. Instrumentation and IT structure of the stand

Figure 2 presents a simplified diagram of: signal acquisition, signal analysis and data transfer. The stand is equipped with devices which measure diagnostic signals: vibration acceleration (RMS value) and temperature of the tested bearing. In addition operating parameters like: instantaneous rotation speed of the shaft, instantaneous frequency of power supply and the load force of the tested bearing are measured.

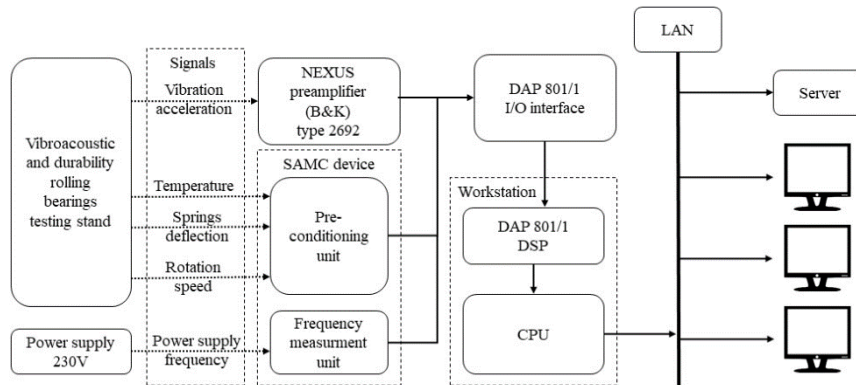


Figure 2. Signal acquisition, signal analysis and data transfer diagram

Signals from tachometer, temperature and optical sensors (springs deflection measurement) are pre-conditioned by a signal acquisition and motor control device (the SAMC device) which is shown in Figure 3. The signal of vibration acceleration is amplified and filtered using anti-aliasing filters in NEXUS preamplifier (B&K) type 2692. The signal acquisition module included in the SAMC device is responsible for tachometer, optical sensor and temperature signals' adjustment to analog-to-digital converter's (ADC) input range 5V and low-pass filtering of these signals (noise reduction). The SAMC device is necessary for input protection of digital signal processor (DSP). It also enables manual or external electric motor control using digital signal from DSP. All signals are transferred to a DSP I/O interface of DAP 801/1.

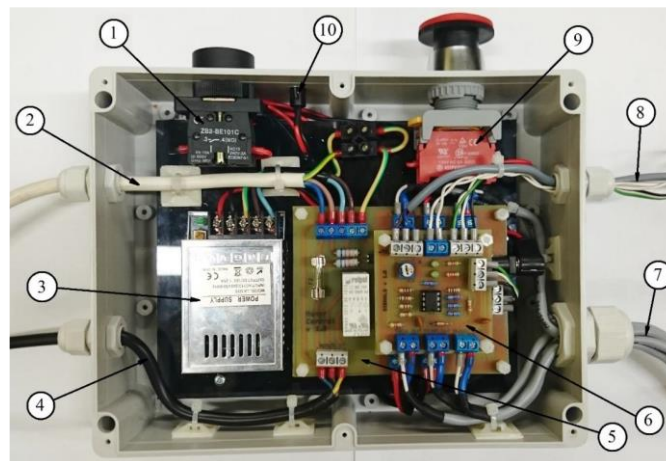


Figure 3. Signal acquisition and motor control device (1 – power switch, 2 – 230 V power supply, 3 – 12 V power supply, 4 – motor supply, 5 – motor control unit with power supply frequency measurement unit, 6 – signal conditioning unit, 7 – signal outputs, 8 – signal inputs, 9 – emergency stop, 10 – LED indicator)

While choosing digital signal processor the following features and parameters of DSP have been taken under consideration: ADC resolution, maximum sampling frequency, number of digital and analog input and output channels, price and device availability. Due to this parameters the DAP 801/1 (Microstar Laboratories) signal processor has been chosen. This DSP is a board which can be mounted in a workstation. Its basic parameters are presented in Table 2 [10].

Table 2. Basic parameters of DAP 801/1 signal processor

ADC resolution	12 bits
ADC sampling frequency	105 kHz
Analog input voltage ranges	-2,5 to +2,5V 0 to 5V -5 to +5V -10 to +10V
Number of analog input channels	8
Number of digital input/output channels	8/8

The sampling frequency (105 kHz) is high enough to observe bearings degradation in higher frequencies about 50 kHz. Due to that the assessment of rolling bearings condition using the SPM method is also possible.



Figure 4. Measurement and control panel of data acquisition and analysis application for the rolling bearings testing stand

The stand is equipped with data acquisition and analysis application. The software was made in DASyLab (Data Acquisition System Laboratory) programming environment and it controls DAP 801/1 signal processor [11, 12]. A screenshot of the measurement and

control panel is presented in Figure 4. The elaborated application can visualize results of measurements as numerical data or in diagrams. The slip of asynchronous motor can be calculated using precisely measured instantaneous rotation speed of the shaft and the power supply frequency. The slip is indirect measure of load moments of the tested rolling bearing. Optionally vibration acceleration and velocity signals and their spectra can be presented as diagrams. The measuring system displays current RMS value of vibration velocity according to PN ISO 10816-1 standard [13]. There is also a possibility to set an alarm thresholds for RMS vibration acceleration, temperature and rotation speed. After one of the thresholds is exceeded system can automatically finish measurements and turn off the drive unit using digital control signal which is sent to the SAMC device. The rolling bearings testing stand may work without human direct supervision and it gives a possibility to carry out long-term researches.

The workstation with DAP 801/1 signal processor is connected to LAN and to data server. Results of measurements and analyses transferred to the server create data libraries. This data can be read by other workstations connected to LAN.

5. Conclusions and remarks

The carried out tests confirm that: the stand is fully functional and fulfils the project assumptions. Necessary corrections and adjustments were introduced during the first test. The experiment was carried out from the brand-new state of the bearing to the vibration phase of its technical degradation. With radial load equal to 1000 N and shaft rotation speed of 3000 RPM the bearing shall be completely degraded in about 3 months. The length of this experiment allows tracking the development of damages in vibroacoustic signals and forming symptom life curves of rolling bearings.

The stand for vibroacoustic and durability rolling bearings testing may be an alternative for professional industrial devices for bearings' long-term durability tests and it can be applied in e.g. didactical process performed in vibroacoustics and technical diagnostics laboratory. This stand provides precise measurements and autonomic work which is necessary in long-term researches. Compact construction of the stand containing overload protection system and automatic turn off system, activated after exceeding limit values of operating parameters or diagnostic signals, allows autonomic work without frequent human supervision. The data obtained from the stand will be used in future researches.

Acknowledgment

The results presented are results of the research that was partially funded with grant 02/21/DSPB/3494 for education allocated by the Ministry of Science and Higher Education of the Republic of Poland.

References

1. SKF Group, *Bearing designs – bearing testing*, Railway Technical Handbook, **1** (2012) 99 – 105.
2. B. Żółtowski, C. Cempel, *Inżynieria diagnostyki maszyn*, ITS Radom 2004.

3. T. Sundström, SPM Instrument AB, *An introduction to the SPM HD method*, SPM Instrument AB Strängnäs 2010.
4. T. Williams, X. Ribadeneira, S. Billington, T. Kurfess, *Rolling Element Bearing Diagnostics In Run-To-Failure Lifetime Testing*, Mechanical Systems and Signal Processing, **15** (2001) 979 – 993.
5. R. B. Randall, J. Antoni, *Rolling element bearing diagnostics – A tutorial*, Mechanical Systems and Signal Processing, **25** (2010) 485 – 520.
6. R. B. Randal, *Vibration-based Condition Monitoring: Industrial, Aerospace and Auto-motive Applications*, Wiley New Delhi 2011.
7. A. Gałęzia, R. Barczewski, B. Jakubek, *Possibilities of faults detection of rolling bearings using energetic descriptors of vibrations signals*, Advances in Condition Monitoring of Machinery in Non-Stationary Operations: Proceedings of the 5th International Conference on Condition Monitoring of Machinery in Non-stationary Operations, Gliwice 2016.
8. M. Wróbel, *Opracowanie systemu akwizycji i analizy sygnałów dla stanowiska do testowania łożysk tocznych*, Politechnika Poznańska 2016.
9. H. Mehdigholi, H. Rafsanjani, M. Behzad, *Estimation of rolling bearing life with damage curve approach*, Polish Maritime Research, **18** (2011) 66 – 70.
10. Microstar Laboratories, Inc., *DAP 800 Manual Installation Guide and Connector Reference Version 1.0*, Washington 1985.
11. National Instruments, *DASYLab Hands On Guide, Book 3*, National Instruments Austin 2002.
12. National Instruments, *DASYLab Data Acquisition, Controlling and Monitoring*, National Instruments Austin 2013.
13. PN ISO 10816-1, *Drgania mechaniczne – Ocena drgań maszyny na podstawie pomiarów na częściach niewirujących – Wytyczne ogólne*.

Large Amplitude Free Vibration Analysis of Tapered Timoshenko Hinged-Hinged Beam Using Coupled Displacement Field Method

Korabathina RAJESH

*Ph.D.Student, Jawaharlal Nehru Technological University,
Kakinada, AP, India, -533003, krajeshmech1112@gmail.com*

Koppanati Meera SAHEB

*Professor, Jawaharlal Nehru Technological University,
Kakinada, AP, India, -533003, meera.aec@gmail.com*

Abstract

Tapered beams are more efficient compared to uniform beams as they provide a better distribution of mass and strength and also meet special functional requirements in many engineering applications like architecture, aeronautical, civil, mechanical, automobile, nuclear and robotics. The authors proposed a new method called Coupled Displacement Field (CDF) method in which the displacement field such as total rotation is assumed such that the assumed displacement must satisfy the kinematic and force boundary condition of the beam. The lateral transverse displacement is derived from the coupling equation which is derived from the static equilibrium conditions of the beam. By the application of principle of minimum total potential energy for different beam boundary conditions, the fundamental frequency parameter value is calculated in terms of taper ratio and slenderness ratio for various maximum amplitude ratios of the tapered Timoshenko shear flexible hinged-hinged beam boundary condition.

Keywords: large amplitude free vibrations, Coupled Displacement Field method, tapered Timoshenko beams, slenderness ratio; taper ratio

1. Introduction

Many authors developed different methods to find the free vibration behaviour of shear flexible beams for a long period of time and are mentioned below. The free vibration of nonuniform beams with general shape and arbitrary boundary conditions was analyzed [1]. Free vibrations of tapered beams with general boundary condition is evaluated by using the ordinary differential governing equation of beams which can be solved by numerical methods and the natural frequencies are calculated by combining the Runge Kutta method and the determinant search method [2]. The dynamic behaviour of beams with linearly varying cross-section was studied by the equation of motion in terms of Bessel functions, and the boundary conditions lead to the frequency equation which is a function of four flexibility coefficients [3]. Natural vibration frequencies of tapered beams by using Euler-Bernoulli beam theory in the presence of an arbitrary number of rotationally, axially and elastically flexible constraints were studied by the dynamic analysis, performed by means of the so-called cell discretization method (CDM), according to which the beam is reduced to a set of rigid bars, linked together by elastic sections, where the bending stiffness and the distributed mass of the bars is concentrated [4]. Wentzel, Kramers, Brillouin (WKB) approximation was used to study the transverse free vibration of a class of variable-cross-

section beams in which the governing equation of motion of the Euler–Bernoulli beam including axial force distribution is utilized to obtain a singular differential equation in terms of the natural frequency of vibration and a WKB expansion series is applied to find the solution [5]. Green’s function method was used for the free vibration problem of non uniform Bernoulli-Euler beams, to find the Green’s function of the fourth order differential operator, occurring at the beam’s equation of motion, the power series method is proposed [6]. The differential transformation method (DTM) was used for free vibration analysis of beams with uniform and non-uniform cross sections [7].

The Coupled Displacement Field method applied to free vibration analysis of uniform Timoshenko beams for different beam boundary conditions [8]. The vibrations of an isotropic beam with a variable cross-section is studied by using the governing equation by reducing it to an ordinary differential equation in spatial coordinate for a family of cross-section geometries with exponentially varying width [9]. Non-linear vibration analysis was premeditated by establishing equations of motion for taper Timoshenko beams [10]. A mathematical model for vibrations of non-uniform flexural beams was presented for free vibrations of non-uniform viscoelastic flexural beams by getting an analytical solution for the fourth order differential equation of beam vibration under appropriate boundary conditions by factorization and calculated mode shapes and damped natural frequencies of the beam for wide range of beam characteristics [11]. The concept of coupled displacement method was successfully applied for large amplitude free vibrations of shear flexible beams and the approach leads to only one undetermined coefficient, in the case of single-term admissible functions, which can easily be used in the principle of conservation of total energy, neglecting damping, to solve the problem [12]. The natural frequencies and dynamic behaviour vibration of linearly tapered beams subjected to different combinations of edge supports by finite element algorithmic procedures are evaluated [13]. The Green’s function method is used in frequency analysis of a beam with varying cross section for the beam carrying an arbitrary number of attached discrete systems. The exact solution of the problem concerns a beam with quadratically varying cross-section area [14]. The vibrational characteristics of tapered beams with continuously varying rectangular cross-section of depth and breadth proportional to x_s and x_t respectively, where both s and t are arbitrary real numbers for a truncated beam and arbitrary positive numbers for a sharp ended beam and x is the axial co-ordinate measured from the sharp end of the beam and obtained the eigen frequency equation by the Rayleigh-Ritz method [15].

The solution for the large amplitude free vibration problems using energy method involves assuming suitable admissible functions for lateral displacement and the total rotation which leads to two coupled nonlinear differential equations in terms of lateral displacement and the total rotation. This can be overcome with less computational efforts by Coupled Displacement Field method in which lateral displacement and total rotation are coupled through the static equilibrium equation of the shear flexible beam.

2. Coupled Displacement Field (CDF) method

The concept of coupled displacement field method is explained in detail. In the Coupled Displacement Field Method (CDF) with the single term admissible function for total rotation θ , the function for transverse displacement w is derived using the coupling equation. The coupling equation has been derived from the kinematic and static boundary conditions of beam.

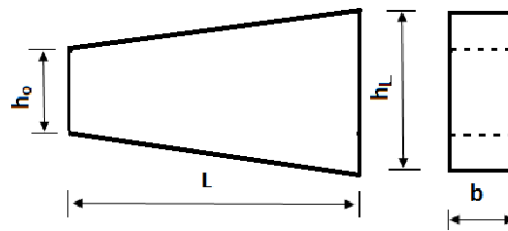


Figure 1. Tapered Timoshenko beam with linearly varying height (depth)

2.1. Coupling equation

From the kinematics of a shear flexible beam theory

$$\bar{u}(x, z) = z\theta \tag{1}$$

$$\bar{w}(x, z) = w(x, z) \tag{2}$$

where \bar{u} is the axial displacement and \bar{w} is the transverse displacements at an any point of the beam, z is the distance of the any point from the neutral axis and θ is the total rotation anywhere on the beam axis and x, z are the independent spatial variables. The axial and shear strains are given by

$$\epsilon_x = z \frac{\partial \theta}{\partial x} \tag{3}$$

$$\gamma_{xz} = \frac{\partial w}{\partial x} + \theta \tag{4}$$

Now, the expressions for the strain energy ‘ U ’ and the work done ‘ W ’ by the externally applied loads are given by

$$U = \frac{EI}{2} \int_0^L \left(\frac{d\theta}{dx} \right)^2 dx + \frac{kGA}{2} \int_0^L \left(\frac{dw}{dx} + \theta \right)^2 dx \tag{5}$$

$$W = \int_0^L p(x)w(x)dx \tag{6}$$

where EI is the flexural rigidity, GA is the shear rigidity, k is the shear correction factor (taken as $5/6$ in the present study), $p(x)$ is the static lateral load per unit length acting on the beam, E is the Young's modulus, G is the shear modulus, x is the axial coordinate and L is the length of the beam. Applying the principle of minimization of total potential energy, as

$$\delta(U - W) = 0 \tag{7}$$

The following equilibrium equations can be obtained

$$kGA \left(\frac{d^2w}{dx^2} + \frac{d\theta}{dx} \right) + p = 0 \tag{8}$$

$$EI \frac{d^2\theta}{dx^2} - kGA \left(\frac{dw}{dx} + \theta \right) = 0 \tag{9}$$

where θ is total rotation, w is transverse displacement. Equations (8) and (9) are coupled equations and can be solved for obtaining the solution for the static analysis of the shear deformable beams. A close observation of equation (8) shows that it is dependent on the load term p and equation (9) is independent of the load term p . Hence, equation (9) is used to couple the total rotation θ and the transverse displacement w , so that the two undetermined coefficients problem (for single term admissible function) becomes a single undetermined coefficient problem and the resulting linear free vibration problem becomes much simpler to solve.

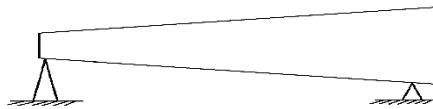


Figure 2. Tapered Timoshenko hinged-hinged beam (depth taper) with axially immovable ends

An admissible function for tapered Timoshenko hinged-hinged beam θ which satisfies all the applicable boundary conditions and the symmetric condition is assumed in the beam domain as

$$\theta = a \frac{\pi}{L} \cos\left(\frac{\pi}{L} x\right) \tag{10}$$

$$\frac{d\theta}{dx} = -a \frac{\pi^2}{L^2} \sin\left(\frac{\pi}{L} x\right) \tag{11}$$

$$\frac{d^2\theta}{dx^2} = -a \cos\left(\frac{\pi}{L}x\right) \frac{\pi^3}{L^3} \quad (12)$$

where a is the central lateral displacement of the beam which is also the maximum lateral displacement. Rewriting equation (9)

$$\frac{dw}{dx} = -\theta + \frac{EI}{kGA} \frac{d^2\theta}{dx^2} \quad (13)$$

By integrating the above equation, lateral displacement can be obtained as

$$w = -a \left[1 + \frac{\pi^2}{L^2} \frac{EI}{kGA} \right] \sin\left(\frac{\pi}{L}x\right) \quad (14)$$

It may be noted here that because of the coupled displacement field concept, the transverse displacement w distribution contains the same undetermined coefficient a as the θ distribution and satisfies all the applicable essential boundary and symmetric conditions.

$$w(0) = w(L) = \left. \frac{dw}{dx} \right|_{x=L/2} = 0 \quad (15)$$

2.2. Linear free vibrations

Linear free vibrations can be studied, once the coupled displacement field for the lateral displacement w , for an assumed θ distribution is evaluated using the principle of conservation of total energy at any instant of time, neglecting damping, which states that $U + T = \text{constant}$. The expression for U and T are given by

$$U = \frac{E}{2} \int_0^L I \left(\frac{d\theta}{dx} \right)^2 dx + \frac{kG}{2} \int_0^L A \left(\frac{dw}{dx} + \theta \right)^2 dx \quad (16)$$

$$T = \frac{\rho\omega_L^2}{2} \int_0^L A w^2 dx + \frac{\rho\omega_L^2}{2} \int_0^L I \theta^2 dx \quad (17)$$

$$A = A_0 \left(1 + \frac{\alpha}{L}x \right), I = I_0 \left(1 + \frac{\alpha}{L}x \right)^3, \alpha = \frac{(h_L - h_0)}{h_L} \quad (18)$$

where T is the kinetic energy, h_L , h_0 , are the height of the beam at left end $x = 0$ and the right end $x = L$ respectively, A_0 and I_0 are cross sectional area and area moment of inertia at right side, A is the area at any cross section, α is the taper ratio. Substituting equations (11), (13) and (18) in equations (16) and after simplification

$$U = \frac{a^2 EI_0 \pi^2}{2L} \left[(0.5 + 0.0871\alpha^3 + 0.4241\alpha^2 + 0.75\alpha) + 3.12 \frac{\pi^2}{\beta^2} (0.5 + 0.25\alpha) \right] \quad (19)$$

Substituting equations (10), (14) and (18) in equations (17) and after simplification

$$T = \frac{a^2 \rho A_0 \omega_L^2 L^3}{2\pi^2} \cdot \left[\left(1 + 3.12 \frac{\pi^2}{\beta^2} \right)^2 (0.5 + 0.25\alpha) + \frac{\pi^2}{\beta^2} (0.5 + 0.1629\alpha^3 + 0.5759\alpha^2 + 0.75\alpha) \right] \quad (20)$$

By the application of principle of minimum total potential energy principle $\left(\frac{\partial(U-T)}{\partial a} = 0 \right)$ with respect to undetermined coefficient a , the fundamental frequency parameter is obtained and is given as below

$$\lambda = \frac{\rho A_0 \omega_L^2 L^4}{EI_0} \quad (21)$$

$$= \pi^4 \frac{\left[(0.5 + 0.0871\alpha^3 + 0.4241\alpha^2 + 0.75\alpha) + 3.12 \frac{\pi^2}{\beta^2} (0.5 + 0.25\alpha) \right]}{\left[\left(1 + 3.12 \frac{\pi^2}{\beta^2} \right)^2 (0.5 + 0.25\alpha) + \frac{\pi^2}{\beta^2} (0.5 + 0.1629\alpha^3 + 0.5759\alpha^2 + 0.75\alpha) \right]} \quad (22)$$

where λ is the non dimensional fundamental frequency parameter, $\beta = L/r$ (slenderness ratio) and r is radius of gyration for the cross-section of the beam.

3. Large Amplitude free vibrations

For an assumed θ distribution, the coupled displacement field for the lateral displacement w is evaluated, after the lateral displacement w is calculated, the large amplitude free vibrations can be studied using the principle of conservation of total energy at any instant of time neglecting damping.

$$U + T + W = \text{const.} \quad (23)$$

Work done due to large amplitudes

$$W = \frac{T_a}{2} \int_0^L \frac{1}{2} \left(\frac{dw}{dx} \right)^2 dx \tag{24}$$

where w is transverse displacement obtained from coupling equation. From Woinowsky-Krieger equation

$$T_a = \frac{E}{2Lr^2} \int_0^L I_0 \left(\frac{dw}{dx} \right)^2 dx \tag{25}$$

where

$$w = a \sin \frac{\pi x}{L}, \frac{dw}{dx} = \frac{a\pi}{L} \cos \left(\frac{\pi x}{L} \right) \tag{26}$$

T_a is the tension developed in the beam because of large deformations. W is the work done by the tension developed because of large amplitudes, ρ is the mass density. T_a is evaluated in terms of the amplitude ratio (a/r). Substituting the values of w (obtained from coupled displacement field), equation (25) in equation (24) and solving the work done due to large amplitudes becomes

$$W = \frac{EI_0 \pi^2 a^4}{16r^2 L} \frac{(2 - \alpha)(\pi^2 \alpha^2 + 3\alpha^2 - 2\pi^2 \alpha + 2\pi^2)}{8\pi^2} \left(1 + \frac{\pi^2}{L^2} 3.12r^2 \right) \tag{27}$$

Substituting equations (19), (20) and (27) in equation (23) and simplifying, the following form is obtained

$$\dot{a}^2 + a^2 \alpha_1 + a^4 \alpha_2 = \text{const.} \tag{28}$$

where

$$\alpha_1 = \frac{EI_0 2\pi^4}{\rho L^4 A_0} \frac{\left[(0.5 + 0.0871\alpha^3 + 0.4241\alpha^2 + 0.75\alpha) + \frac{3.12\pi^2}{\beta^2} (0.5 + 0.25\alpha) \right]}{\left[\left(1 + \frac{3.12\pi^2}{\beta^2} \right)^2 (0.5 + 0.25\alpha) + \frac{\pi^2}{\beta^2} (0.5 + 0.1629\alpha^3 + 0.5759\alpha^2 + 0.75\alpha) \right]} \tag{29}$$

$$\alpha_2 = \frac{EI_0 \pi^2}{35\rho L^4 A_0 r^2} \frac{\left[(2 - \alpha)(\pi^2 \alpha^2 + 3\alpha^2 - 2\pi^2 \alpha + 2\pi^2) + \left(1 + \frac{3.12\pi^2}{\beta^2} \right)^2 \right]}{\left[\left(1 + \frac{3.12\pi^2}{\beta^2} \right)^2 (0.5 + 0.25\alpha) + \frac{\pi^2}{\beta^2} (0.5 + 0.1629\alpha^3 + 0.5759\alpha^2 + 0.75\alpha) \right]} \tag{30}$$

The ratio of non linear and linear frequency is expressed as

$$\left(\frac{\omega_{NL}}{\omega_L}\right)^2 = 1 + \frac{3}{2} \left(\frac{\alpha_2}{\alpha_1}\right) \left(\frac{a_m}{r}\right)^2 \tag{31}$$

$$\left(\frac{\omega_{NL}}{\omega_L}\right)^2 = 1 + \frac{3}{70\pi^2} \frac{\left[(2-\alpha) \left(\pi^2 \alpha^2 + 3\alpha^2 - 2\pi^2 \alpha + 2\pi^2 \right) \left(1 + \frac{3.12\pi^2}{\beta^2} \right)^2 \right]}{\left[(0.5 + 0.871\alpha^3 + 0.4241\alpha^2 + 0.75\alpha) + \frac{3.12\pi^2}{\beta^2} (0.5 + 0.25\alpha) \right]} \left(\frac{a_m}{r}\right)^2 \tag{32}$$

4. Numerical results and discussion

The concept of coupled displacement field and harmonic balance method are used to determine the ratios of non linear radian frequency ω_{NL} to the linear radian frequency ω_L of tapered Timoshenko beams with the two most practically used hinged-hinged beam boundary condition. Suitable single term trigonometric admissible functions are used to represent the total rotatio θ in the coupled displacement field method. The corresponding coupled lateral displacement w is derived using the coupling equation. The numerical results are obtained in terms of ω_{NL}/ω_L for various maximum amplitude, taper parameter and slenderness ratios. To assess the accuracy of the results, the present results obtained from the coupled displacement filed method are compared with the existing literature. Table.1 shows the variation of linear non dimensional Fundamental frequency parameter with slenderness ratio and taper ratio for hinged-hinged beam boundary condition. For the sake of comparison and validation of the coupled displacement filed method, the same results obtained by the other researchers are also included in Table 1. It is observed from Table 1 that the non dimensional linear fundamental frequency parameter value increases with increase in taper ratio for a given slenderness ratio. It is also observed from Table 1, the non dimensional linear fundamental frequency parameter value increases with increase in slenderness ratio for a given taper parameter. Table 2 Table 3 and Table 4 show the variation of frequency ratio ω_{NL}/ω_L with maximum amplitude and taper parameter for different slenderness ratios such as 20, 50 and 100 are given respectively for hinged-hinged beam boundary condition. It is found from Table 2, Table 3 and Table 4 that frequency ratio is function of three parameters such as maximum amplitude ratio, taper parameter and slenderness ratio. It is in general found from Table 2, Table 3 and Table 4 that frequency ratio increases with increase of maximum amplitude ratio for a given taper parameter and slenderness ratio. It is also observed from Table 2, Table 3 and Table 4 that frequency ratio decreases with increase of taper parameter for a given slenderness ratio and amplitude ratio. This is mainly because of as taper ratio increases mass of the beam also increases.

Table 1. $\lambda^{1/2}$ values for a tapered Timoshenko hinged-hinged beam (depth taper)

α	β							
	10		20		40	80	100	
	CDF Method	Ref.[13]	CDF Method	Ref.[13]	CDF Method	CDF Method	CDF Method	Ref.[13]
0	8.3912	8.388	9.4107	9.411	9.7470	9.8384	9.8496	9.850
0.1	8.6916	8.683	9.8415	9.829	10.2267	10.3317	10.3446	-
0.15	8.8435	-	10.0595	-	10.4695	10.5816	10.5953	-
0.2	8.9962	8.955	10.2789	10.228	10.7141	10.8333	10.8480	-
0.25	9.1496	-	10.4996	-	10.9604	11.0869	11.1024	-
0.3	9.3036	9.205	10.7214	10.610	11.2082	11.3420	11.3585	-
0.35	9.4580	-	10.9443	-	11.4574	11.5987	11.6161	-
0.4	9.6127	-	11.1681	-	11.7079	11.8569	11.8752	-
0.45	9.7676	-	11.3926	-	11.9596	12.1163	12.1356	-
0.5	9.9225	-	11.6178	-	12.2124	12.3770	12.3973	-
0.55	10.0774	-	11.8435	-	12.4661	12.6389	12.6601	-
0.6	10.2321	-	12.0697	-	12.7208	12.9018	12.9241	-
0.65	10.3866	-	12.2962	-	12.9764	13.1658	13.1891	-
0.7	10.5407	-	12.5230	-	13.2327	13.4307	13.4551	-
0.75	10.6943	-	12.7500	-	13.4897	13.6965	13.7219	-
0.8	10.8475	-	12.9771	-	13.7474	13.9631	13.9897	-
0.85	11.0000	-	13.2042	-	14.0057	14.2304	14.2582	-
0.9	11.1519	-	13.4313	-	14.2644	14.4986	14.5274	-
0.95	11.3030	-	13.6583	-	14.5237	14.7673	14.7974	-
1	11.4533	-	13.8852	-	14.7834	15.0368	15.0681	-

Table 2. ω_{NI}/ω_L values for a tapered Timoshenko hinged-hinged beam for $\beta = 20$

a_m/r	$\alpha = 0.25$		$\alpha = 0.5$		$\alpha = 0.75$		$\alpha = 1$	
	CDF Method	Ref.[10]	CDF Method	Ref.[10]	CDF Method	Ref.[10]	CDF Method	Ref.[10]
0.10	1.0009	1.0009	1.0005	1.0007	1.0003	1.0006	1.0002	1.0005
0.20	1.0036	1.0037	1.0019	1.0030	1.0011	1.0025	1.0007	1.0021
0.30	1.0081	-	1.0042	-	1.0025	-	1.0016	-
0.40	1.0144	1.0146	1.0075	1.0119	1.0044	1.0100	1.0028	1.0085
0.50	1.0224	-	1.0118	-	1.0069	-	1.0044	-
0.60	1.0321	1.0325	1.0169	1.0266	1.0099	1.0224	1.0064	1.0190
0.70	1.0434	-	1.0230	-	1.0134	-	1.0087	-
0.80	1.0564	1.0570	1.0299	1.0467	1.0175	1.0394	1.0113	1.0336
0.90	1.0709	-	1.0377	-	1.0221	-	1.0143	-
1.00	1.0868	1.0878	1.0464	1.0721	1.0272	1.0608	1.0177	1.0519
1.10	1.1042	-	1.0559	-	1.0328	-	1.0213	-
1.20	1.1230	1.1239	1.0662	1.1022	1.0389	1.0864	1.0253	1.0740
1.30	1.1430	-	1.0773	-	1.0455	-	1.0297	-
1.40	1.1642	-	1.0891	-	1.0526	-	1.0343	-
1.50	1.1865	1.1878	1.1017	1.1552	1.0602	1.1315	1.0393	1.1131

Table 3. ω_{NL}/ω_L values for slenderness ratio $\beta (L/r) = 50$ for hinged-hinged tapered Timoshenko beam

a_m/r	α			
	$\alpha = 0.25$	$\alpha = 0.5$	$\alpha = 0.75$	$\alpha = 1$
	CDF Method	CDF Method	CDF Method	CDF Method
0.10	1.0005	1.0002	1.0001	1.0000
0.20	1.0018	1.0010	1.0005	1.0004
0.30	1.0041	1.0021	1.0012	1.0008
0.40	1.0073	1.0038	1.0022	1.0014
0.50	1.0114	1.0060	1.0034	1.0022
0.60	1.0164	1.0086	1.0049	1.0032
0.70	1.0222	1.0116	1.0067	1.0043
0.80	1.0290	1.0152	1.0088	1.0056
0.90	1.0366	1.0192	1.0111	1.0071
1.00	1.0450	1.0236	1.0137	1.0088
1.10	1.0542	1.0285	1.0165	1.0106
1.20	1.0642	1.0338	1.0196	1.0127
1.30	1.0750	1.0396	1.0230	1.0148
1.40	1.0865	1.0458	1.0266	1.0172
1.50	1.0987	1.0524	1.0305	1.0197
2	1.1697	1.0914	1.0536	1.0348
3	1.3521	1.1959	1.1170	1.0767
4	1.5724	1.3284	1.2001	1.1327
5	1.8168	1.4815	1.2991	1.2009

Table 4. ω_{NL}/ω_L values for a tapered Timoshenko hinged-hinged beam for $\beta = 100$

a_m/r	α							
	0.25		0.5		0.75		1	
	CDF Method	Ref.[10]						
0.10	1.0010	1.0010	1.0004	1.0008	1.0003	1.0007	1.0002	1.0006
0.20	1.0033	1.0040	1.0017	1.0033	1.0010	1.0028	1.0006	1.0025
0.30	1.0075	-	1.0039	-	1.0022	-	1.0014	-
0.40	1.0132	1.0158	1.0069	1.0132	1.0040	1.0113	1.0025	1.0098
0.50	1.0206	-	1.0107	-	1.0062	-	1.0040	-
0.60	1.0295	1.0353	1.0154	1.0294	1.0089	1.0252	1.0057	1.0219
0.70	1.0400	-	1.0209	-	1.0121	-	1.0078	-
0.80	1.0519	1.0619	1.0272	1.0516	1.0158	1.0444	1.0101	1.0387
0.90	1.0653	-	1.0344	-	1.0199	-	1.0128	-
1.00	1.0800	1.0950	1.0423	1.0795	1.0245	1.0685	1.0158	1.0597
1.10	1.0961	-	1.0509	-	1.0296	-	1.0191	-
1.20	1.1134	1.1344	1.0603	1.1127	1.0351	1.0972	1.0227	1.0849
1.30	1.1319	-	1.0704	-	1.0411	-	1.0266	-
1.40	1.1516	-	1.0813	-	1.0475	-	1.0308	-
1.50	1.1724	1.2033	1.0928	1.1712	1.0543	1.1479	1.0352	1.1296

5. Conclusions

The concept of the Coupled Displacement Field (CDF) method applicable to beams presented in this paper is successfully applied to study the large amplitude free vibration behaviour of tapered Timoshenko beams with axially immovable ends. Elegant and

accurate closed form expression for $\left(\frac{\omega_{NL}}{\omega_L}\right)^2$ for the hinged-hinged beam boundary

condition is obtained in terms of maximum amplitude ratio, taper ratio and slenderness ratio for the assumed single term admissible function for the total rotation θ .

Acknowledgements

The authors would like to thank the authorities of University College of Engineering, Jawaharlal Nehru Technological University Kakinada (JNTUK), for sponsoring and presenting the research paper under TEQIP-II.

References

1. S. Abrate, *Vibration of non-uniform rods and beams*, Journal of Sound and Vibration, **185** (4) (1995) 703 – 716.
2. B. K. Lee et al., *Free vibrations of tapered Beams with general boundary condition*, (KSCE) Journal of Civil Engineering, **6**(3) (2002) 283 – 288.
3. M. A. De Rosa, N. M. Auciello, *Free vibrations of tapered beams with flexible ends*, Computers & Structures, **60**(2) (1996) 197 – 202.
4. M. A. De Rosa, M. Lippiello, *Natural vibration frequencies of Tapered beams*, Engineering Transactions, **57**(1) (2009) 45 – 66.
5. R. D. Firouz-Abadi et al., *An asymptotic solution to transverse free vibrations of variable-section beams*, Journal of Sound and Vibration, **304** (2009) 530 – 540.
6. I. Zamorska, *Free Transverse vibrations of non- Uniform beams*, Scientific Research of the Institute of Mathematics and Computer Science, **9**(2) (2010) 244 – 250.
7. A. A. Mahmoud et al., *Free vibrations of uniform and non uniform Euler beam using differential transformation method*, Asian Journal of Mathematics and Applications, article id ama0097, (2013) 1 – 16.
8. K. Meera Saheb et al., *Free vibration analysis of Timoshenko beams using Coupled Displacement Field Method*. Journal of Structural Engineering, **34** (2007) 233 – 236.
9. M. C. Ece et al., *Vibration of a variable cross-section beam*, Mechanics Research Communications, **34** (2007) 78 – 84.
10. M. Liao, H. Zhong., *Non-linear Vibration Analysis of Taper Timoshenko beams*, Chaos, Solitons and Fractals, **36** (2008) 1267 – 1272.
11. M. H. Taha, S. Abohadima., *Mathematical Model for Vibrations of Non-Uniform Flexural Beams*, Journal of Engineering Mechanics, **15** (1) (2008) 3 – 11.
12. G. V. Rao et al., *Concept of Coupled Displacement Filed for large amplitude free Vibrations of shear flexible beams*, Journal of Vibration and Acoustics (ASME), **128** (2006) 251 – 255.

13. R. E. Rossi, P. A. A. Laura, *Numerical Experiments on Vibrating, Linearly Tapered Timoshenko Beams*, Journal of Sound and Vibration, **168** (1) (1993) 179 – 183.
14. S. Kukla, I. Zamojska., *Application of the Green's function Method in Free Vibration Analysis of Non Uniform Beams*, Scientific Research of the Institute of Mathematics and Computer Science, Issue 1, **4** (2005) 87 – 94.
15. D. Zhou, Y. K. Cheung, *The free vibration of a type of tapered beams*, Computer Methods in Applied Mechanics and Engineering, **188** (2000) 203 – 216.

Theoretical Determination of Wear and Lifetime of the Screen Sowing Surface

Vladimir ZASELSKIY, Dmitry POPOLOV, Igor ZASELSKIY
*Department of metallurgical equipment, Krivoy Rog Metallurgical institute,
National metallurgical academy of Ukraine,
Stepana Tilgi, 5, Krivoy Rog, 50006, Ukraine, dmitrypopolov@gmail.com*

Abstract

In the article researches of wear of polymeric sowing surfaces of vibrating screens are given. The mathematical model was obtained with analytical methods that allow one to describe the effect of the regime and technological parameters of a vibrating screen, as well as the physical properties of the material being transported, on the wear of a polymeric sowing surface. The obtained equations allow us to determine the lifetime of a surface made of polymer, taking into account the wear of the contact surface, as well as the change in the size of the sieve aperture.

Keywords: polymer, sowing surface, wear, vibrating screen

1. Introduction

Studying of the mechanism and the main regularities of wear of the sowing surface of screen made with the basis of polymers comprised of two tasks: the first is to determine the wear which affects the main dimensions of screen; the second is to determine the maximum lifetime of the product. In the first case, the wear significantly influences the value of the screen natural oscillation, which ensure the screen resonance in case they are equal to the forced oscillations of the screen, which leads to its self-cleaning from the stuck material. In the second one, the lifetime of the screen, apart from the actual forces, depends directly on the physico-mechanical characteristics of polymer itself.

Today, a lot of researches are devoted to the wear of polymers [1-3]. For the vibrating screens sowing surfaces made from the mentioned materials, however, these questions haven't been studied sufficiently.

2. Materials and methods

By the nature of the main process, the wear of the sowing surface made of polymers can be divided into abrasive and fatigue. During the evaluating of the polymers abrasive wear the power criterion is often used (the product of the pressure on the sliding speed). In case the pressure is constant, the wear depends on the sliding speed. In other researches devoted to the wear of work tool determination during the material vibration transmission [4, 5], it is established that the specific work value of the frictional forces A_f on the contact 'sowing surface-charge material', during the oscillation period T , is also proportional to the sliding speed:

$$A_f = \int_0^T F(t) \cdot \dot{\xi}_1(t) dt \quad [\text{J/m}^2], \tag{1}$$

Where $F(t)$ is the instantaneous value of the abrasive material specific frictional force on contact with the sowing surface $[\text{N/m}^2]$; $\dot{\xi}_1(t)$ instantaneous speed of relative slip of the material, $[\text{m/s}]$.

So, considering expression (1), the main task is to determine the material frictional forces at the contact with the sowing surface, and also to determine the material's relative slippage. Taking into account all the factors of vibration influence during the calculation of these parameters is extremely difficult. In order to avoid considering the material layer internal forces, we shall use the following assumptions:

- the dependence of the amplitudes damping of vertical and horizontal oscillations in the layer is exponential and in the frequency band $\omega = 70, \dots, 120 \text{ [s}^{-1}\text{]}$ retains constant values;
- when the material slips at any moment, the frictional force is determined by the Coulomb's law (in our case it is permissible, because the temperature regime is constant and does not exceed $50 \text{ }^\circ\text{C}$ on the average)

$$F(t) = \frac{f \cdot N(t)}{S_s - S_h} \quad [\text{N/m}^2], \tag{2}$$

where f is the friction coefficient; $N(t)$ is the sowing surface normal reaction, $[\text{N}]$; S_s is the area of the sowing surface, $[\text{m}^2]$; S_h is the area of the holes in the sowing surface, $[\text{m}^2]$.

3. Mathematical modeling of wear and lifetime of the sowing surface

Let's consider the volume movement of the element of a layer of material in reference to the sowing surface inclined at an angle to the horizon and oscillating along a circular trajectory (Figure 1).

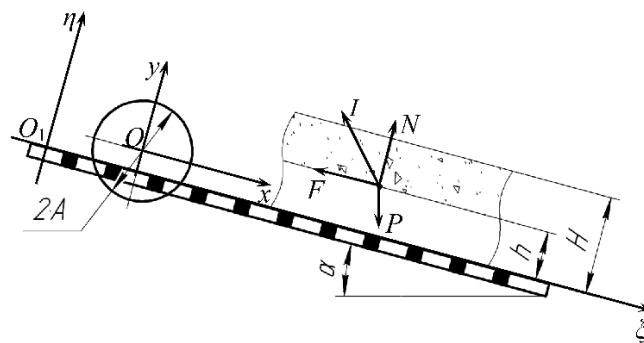


Figure 1. Analytical model

In the fixed xOy coordinate system, the equation of the trajectory of the points displacement of the sowing surface in the parametric form is

$$\begin{cases} x(t) = A \cdot \cos(\omega t) \\ y(t) = A \cdot \sin(\omega t) \end{cases} \text{ [m]}, \tag{3}$$

where A is the oscillation amplitude, [m]; ω is the oscillation frequency, [s⁻¹].

Projections of the absolute movement of material at height h , taking into account the assumed admission of the damping of oscillations law in the absence of relative slip of material over a vibrating sowing surface:

$$\begin{cases} x(h) = x \cdot e^{-\beta_t \cdot h} = A \cdot \cos(\omega t) \cdot e^{-\beta_t \cdot h} \\ y(h) = y \cdot e^{-\beta_l \cdot h} = A \cdot \sin(\omega t) \cdot e^{-\beta_l \cdot h} \end{cases} \text{ [m]}, \tag{4}$$

where β_t and β_l are the transverse and longitudinal oscillations attenuation coefficients in the charge material layer respectively, [m⁻¹] [6].

In the moving coordinate system $\eta O_1 \xi$ associated with the oscillating sowing surface, the relative motion of a layer, equations of material of thickness $H - h$ located at the height h from the plane of the sowing surface in the absence of its slipping or tearing will be

$$\begin{cases} m \cdot \ddot{\xi} = m \cdot g \cdot \sin \alpha - m \cdot \ddot{x}(t) - F(t, h) \\ m \cdot \ddot{\eta} = -m \cdot g \cdot \cos \alpha + m \cdot \ddot{y}(t) + N(t, h) \end{cases} \tag{5}$$

where m is the mass of material in a layer of thickness $H - h$, [kg]; $F(t, h)$ and $N(t, h)$ are the frictional force and the regular reaction at height h respectively, [N]; $\ddot{\xi}$ and $\ddot{\eta}$ are the average relative accelerations of the material layer, [m/s²].

Taking into account (3), considering the assumption (2), the system (5) takes following form

$$\begin{cases} m \cdot \ddot{\xi} = m \cdot g \cdot \sin \alpha + m \cdot A \cdot \omega^2 \cdot \cos(\omega t) - f \cdot N(t, h) \\ m \cdot \ddot{\eta} = -m \cdot g \cdot \cos \alpha - m \cdot A \cdot \omega^2 \sin(\omega t) + N(t, h) \end{cases} \tag{6}$$

The average relative accelerations in the material $\ddot{\xi}$ and $\ddot{\eta}$ layer are obtained by integrating the relative acceleration of the material in reference to the height h in the range from h to H :

$$\ddot{\xi} = \frac{1}{H - h} \cdot \int_h^H \frac{d^2 x(h)}{dt^2} dh + \frac{d^2 x(t)}{dt^2}; \tag{7}$$

$$\ddot{\eta} = \frac{1}{H-h} \cdot \int_h^H \frac{d^2 y(h)}{dt^2} dh + \frac{d^2 y(t)}{dt^2}. \tag{8}$$

Taking into account (3) and (4) the expression (7) and (8) will take the form of

$$\ddot{\xi} = \frac{A \cdot \omega^2}{(H-h) \cdot \beta_l} \cdot \cos(\omega t) \cdot (e^{-\beta_l \cdot H} - e^{-\beta_l \cdot h}) - A \cdot \omega^2 \cdot \cos(\omega t) \text{ [m/s}^2\text{]}; \tag{9}$$

$$\ddot{\eta} = \frac{A \cdot \omega^2}{(H-h) \cdot \beta_l} \cdot \sin(\omega t) \cdot (e^{-\beta_l \cdot H} - e^{-\beta_l \cdot h}) - A \cdot \omega^2 \cdot \sin(\omega t) \text{ [m/s}^2\text{]}. \tag{10}$$

Substituting (10) into (6), we determine the expressions for the force of a regular reaction at the time when the material is on a vibrating sowing surface, expressing the mass of material in the layer as

$$m = \rho \cdot S \cdot (H-h) \text{ [kg]}, \tag{11}$$

where ρ is the bulk density of material, [kg/m³]; S is the material layer base area, [m²]; $H-h$ is the height of layer, [m]

$$N(t, h) = \rho \cdot S \cdot (H-h) \cdot g \cdot \cos \alpha + \frac{\rho \cdot S \cdot A \cdot \omega^2}{\beta_l} \cdot \sin(\omega t) \cdot (e^{-\beta_l \cdot H} - e^{-\beta_l \cdot h}). \tag{12}$$

In the slip phase, the movement of the material layer is described by the first equation of the system (6), characterized by the acceleration $\ddot{\xi}$ which is the average acceleration of the layer in the presence of slip, and the normal reaction $N(t, h)$ takes the corresponding value $h = 0$. Since the material is in contact with the perforated screening surface, it is necessary to take into account its clean opening with the aid of the coefficient

$$K_{co} = \frac{S_h}{S_s}, \tag{13}$$

where K_{co} is the coefficient of the clear opening of the seeding surface.

Taking into account the aforementioned, the first equation of system (6) and expression (12) take following form

$$m \cdot \ddot{\xi}_1 = m \cdot g \cdot \sin \alpha + m \cdot A \cdot \omega^2 \cdot \cos(\omega t) - f \cdot N(t) \text{ [N]}, \tag{14}$$

$$N(t) = \left[\rho \cdot S \cdot H \cdot g \cos \alpha + \frac{\rho \cdot S \cdot A \cdot \omega^2}{\beta_l} \cdot \sin(\omega t) \cdot (e^{-\beta_l \cdot H} - 1) \right] \cdot (1 - K_{co}) \text{ [N]}. \tag{15}$$

The frictional forces at the slippage time are equal to the maximum possible and they are determined by the relations

$$F = \begin{cases} -f \cdot N & \text{if } \ddot{\xi}_1 > 0 \\ f \cdot N & \text{if } \ddot{\xi}_1 < 0 \end{cases} \quad (16)$$

Putting (11) and (15) into expression (14), taking into account condition (16), we obtain the expression for determining the average acceleration of the layer in the presence of slippage

$$\begin{aligned} \ddot{\xi}_1(t)_{\pm} = & g \cdot \sin \alpha + A \cdot \omega^2 \cdot \cos(\omega t) \pm f \cdot g \cdot \cos \alpha \cdot (1 - K_{co}) \pm f \cdot \frac{A \cdot \omega^2}{\beta_l \cdot H} \cdot \sin(\omega t) \times \\ & \times (e^{-\beta_l \cdot H} - 1) \cdot (1 - K_{co}) \text{ [m/s}^2\text{]}. \end{aligned} \quad (17)$$

By integrating (17) we get the relative speed of material with slipping that takes the following form on rearrangement

$$\begin{aligned} \dot{\xi}_1(t)_{\pm} = & \int \ddot{\xi}_1(t) dt = g \cdot t \cdot \sin \alpha + A \cdot \omega \cdot \sin(\omega t) \pm f \cdot t \cdot g \cos \alpha \cdot (1 - K_{co}) \\ & \mp f \cdot \frac{A \cdot \omega}{\beta_l \cdot H} \times \cos(\omega t) \cdot (e^{-\beta_l \cdot H} - 1) \cdot (1 - K_{co}) + C \text{ [m/s]}. \end{aligned} \quad (18)$$

The integration constant is found from the initial conditions

$$\dot{\xi}_1(t^*) = \dot{\xi}_1^*, \quad (19)$$

where $\dot{\xi}_1^*$ is the initial velocity of the material layer in the slip phase, [m/s].

Then the expression (18) takes the form

$$\begin{aligned} \dot{\xi}_1(t)_{\pm} = & g \cdot \sin \alpha \cdot (t - t^*) + A \cdot \omega \cdot (\sin(\omega t) - \sin(\omega t^*)) \pm f \cdot g \cdot \cos \alpha \cdot (1 - K_{co}) \\ & \times (t - t^*) \mp f \cdot \frac{A \cdot \omega}{\beta_l \cdot H} \cdot (e^{-\beta_l \cdot H} - 1) \cdot (1 - K_{co}) \cdot (\cos(\omega t) - \cos(\omega t^*)) + \dot{\xi}_1^* \text{ [m/s]}. \end{aligned} \quad (20)$$

Taking into account (15) and (2) the instantaneous value of the abrasive material specific frictional force on contact with the sowing surface will be:

$$\begin{aligned} F(t) = & \left[f \cdot (1 - K_{co}) \cdot \left[\rho \cdot H \cdot S \cdot g \cdot \cos \alpha + \frac{\rho \cdot S \cdot A \cdot \omega^2}{\beta_l} \right. \right. \\ & \left. \left. \times \sin(\omega t) \cdot (e^{-\beta_l \cdot H} - 1) \right] \right] / (S_s - S_h) \text{ [N/m}^2\text{]}. \end{aligned} \quad (21)$$

Substituting (20) and (21) into expression (1) and integrating at the sliding stage from δ_+ to φ_+ , and at the stage of sliding back from δ_- to φ_- , we obtain the specific work of the frictional force on the contact sowing surface charge material

$$A_f = \int_{\delta_+}^{\varphi_+} F(t) \cdot \dot{\xi}_+(t) dt - \int_{\delta_-}^{\varphi_-} F(t) \cdot \dot{\xi}_-(t) dt \text{ [J/m}^2\text{]}. \quad (22)$$

Knowing the specific work of frictional forces A_f during the oscillation period, we can find the specific work of friction during the operation of the screen during τ hours

$$A_\tau = 3600 \cdot A_f \cdot \frac{\omega}{2 \cdot \pi} \cdot \tau \text{ [J/m}^2\text{]}. \quad (23)$$

Then the wear value at the contact "sowing surface - material" can be defined as

$$I = K_e \cdot A_\tau \text{ [m]}, \quad (24)$$

where K_e is the coefficient determined experimentally for the interacting pair "sowing surface - material", [m³/J].

The obtained formulas make it possible to determine the wear of the sieve by the height of its surface, but, in addition to surface wear, wear occurs the walls of the sieve holes, too. The reason of the walls wear of the sieve holes is the interaction of the flow of particles passing through it. When the wear of the walls occurs only due to frictional forces on the contact "material hole of the screen" (in our case, the impact forces are neglected), the value of such wear can be determined as for the sowing surface by the formula (1). Only in this case the normal reaction of the walls to the material in accordance with [4] will be determined as

$$N' = \frac{m_0 \cdot A \cdot \omega^2 \cdot \cos \alpha}{P \cdot h_{s,t}} \text{ [N/m}^2\text{]}, \quad (25)$$

where P is the hole's perimeter, [m]; $h_{s,t}$ is the screen's thickness, [m]; m_0 is the mass of particles in the hole, which is defined as

$$m_0 = \frac{q \cdot h_{s,t}}{n \cdot \sqrt{2 \cdot g \cdot h_{s,t}}} \text{ [kg]}, \quad (26)$$

where q is the flow of material passing through the unit of the screen area per unit time; n is the number of holes per unit area of the screen.

The specific frictional force of the material against the wall of the sieve hole in this case will be

$$F' = N' \cdot f = \frac{m_0 \cdot A \cdot \omega^2 \cdot \cos \alpha}{P \cdot h_{s,t}} \cdot f \text{ [N/m}^2\text{]}. \quad (27)$$

In this formula, the friction coefficient is assumed to be the same as in the case of determining the frictional force for surface wear. The average slip velocity of the material relative to the wall surface in our case will be

$$V_s = \frac{1}{2} \cdot \sqrt{2 \cdot g \cdot h_{s,t}} + A \cdot \omega \quad [\text{m/s}]. \quad (28)$$

Substituting (27) and (28) in (1), we will be able to determine the specific work of the forces of A'_f dry friction at the contact of the screen hole surface with the material during the oscillations period $\omega/(2 \cdot \pi)$

$$A'_f = \left[\frac{m_0 \cdot A \cdot \omega^2 \cdot \cos \alpha}{P \cdot h_{s,t}} \cdot f \cdot \left(\frac{1}{2} \cdot \sqrt{2 \cdot g \cdot h_{s,t}} + A \cdot \omega \right) \right] \cdot \frac{\omega}{2 \cdot \pi} \quad [\text{J/m}^2]. \quad (29)$$

Then the friction work during the screen operation during hours by analogy with (23) can be defined as

$$A'_\tau = 3600 \cdot A'_f \cdot \frac{\omega}{2 \cdot \pi} \cdot \tau \quad [\text{J/m}^2]. \quad (30)$$

The wear value of the sowing surface walls of the screen is determined by taking into account (29) and (30) as

$$I' = K_e \cdot A'_\tau \quad [\text{m}]. \quad (31)$$

During the studying of the sowing surface of the screen made of polymer, determining the wear of its surface and walls is important when we chose dynamic screening parameters that allow it to provide resonant oscillations due to frequency regulation (which leads to better screening efficiency due to a decrease in the screening capacity of the screen), however it doesn't provide an opportunity to determine the term of its lifetime.

To determine the life (necessary at the design stage) of a surface made of polymer, it is possible to calculate the limiting number of deformation cycles n' of its surface layers in accordance with [1], starting from the fatigue failure of the material:

$$n' = \left(\frac{\sigma_0 \cdot \varphi}{3 \cdot f \cdot P_1} \right)^{t_{d,e}}, \quad (32)$$

where σ_0 is the polymer strength [Pa]; φ is the relative area of the actual contact is equal to the ratio of the area of the actual contact S_a to the S_n nominal contact, i.e. $\varphi = S_a/S_n$; f is the friction coefficient; P_1 is the material pressure on the contact area, equal to $P_1 = N(t, h)$, [N/m²]; $t_{d,e}$ dynamic endurance coefficient of the material (determined experimentally in $\ln \delta - \ln n'$ coordinates).

4. Conclusions

So, (24), (31), (23) and (30) entering into them (with allowance of (32)) are the mathematical model to determine of engineering characteristics basis the polymer sowing surfaces of the screen, taking into account the mode and technological characteristics of the vibration machine, the peculiarity of this technique is that when assessing the operating time of the gray surface for failure, based on fatigue failure of the material, the wear is not only superficial layers, but also the change in the cross-section of the holes of the sowing surface.

The method was based on a phenomenological model in which the intralayer power of the charge material takes into account the damping factors of the oscillations in it, which allows one to take into account the features of the vibration displacement of the layers along the plane making circular plane-parallel oscillations.

References

1. G. M. Bartenev, V. V. Lavrent'ev, *Friction and wear of polymers*, Khimiya Publ., Leningrad 1972.
2. V. V. Grib, G. E. Lazarev, *Laboratory testing of materials for friction and wear*, Nauka Publ., Moscow 1968.
3. V. A. Belyy, A. I. Sviridenok, M. I. Petrokovets, V. G. Savkin, *Friction and wear of materials based on polymers*, Nauka i tekhnika Publ., Minsk 1976.
4. A. D. Uchitel, V. V. Severnyuk, V. P. Lyalyuk, V. I. Bolshakov, *Sorting of mineral raw materials and charge on vibrating screens*, Porogi Publ., Dnepropetrovsk 1998.
5. L. Yu. Brener, *Creation of noncentro-mass vibrating feeders for charge conveying systems for blast furnaces of large volume*, PhD Diss., Krivoy Rog 1982.
6. A. D. Uchitel, V. V. Guschin, *Vibrational output of rock mass*, Nauka Publ., Moscow 1981.

The Influence of the Cutting Tooth Design and Wear of a Saw Chain on the Vibration Level of a Chainsaw

Wojciech RUKAT

Poznan University of Technology, Faculty of Mechanical Engineering and Management, 60-965 Poznan, 3 Piotrowo St, Poland, wojciech.rukat@put.poznan.pl

Bartosz JAKUBEK

Poznan University of Technology, Faculty of Mechanical Engineering and Management, 60-965 Poznan, 3 Piotrowo St, Poland, bartosz.jakubek@put.poznan.pl

Abstract

Chainsaws are the most basic mechanical tools used to harvest and pre-treat wood. Unfortunately, these devices emit noise and vibrations exceeding the maximum permissible levels for an 8-hour working day. Many factors influence the level of noise and vibration emitted by chainsaws. Since the conscious choice of the saw chain can significantly contribute to: productivity increase, vibration reduction and the operator's permissible total exposure time extension the influence of the type of a cutting tooth and its wear on the vibration level recorded on the handles of the device has been investigated in this paper.

Keywords: chainsaw, saw chain wear, cutting tooth design, local vibrations

1. Introduction

Currently, a wide range of devices equipped with an independent internal combustion engine is available on the market. A chainsaw is the most basic device in the forest and wood industry. The greatest risk for operators, connected with the use of a chainsaw, are the vibration and acoustic impacts.

One of requirements for admission of a device to EU market is the manufacturer's declaration concerning the intensity of the harmful agents and other hazards. The vibration levels declared by the manufacturers are determined for strictly defined, standardized conditions [1-4]. The level of vibration is determined basing on equation (1). Furthermore, for each of the operating states, a share of 1/3 of the total operating time of the device was assumed [1, 2].

$$a_{hv,eq} = \sqrt{\frac{1}{3}(a_{hv,ID}^2 + a_{hv,FL}^2 + a_{hv,RA}^2)} \quad (1)$$

Where: $a_{hv,eq}$ – equivalent vibration level, $a_{hv,ID}$ – vibration level measured while idle speed, $a_{hv,FL}$ – vibration level measured under full load, $a_{hv,RA}$ – vibration level measured while racing.

Equal shares of total operating time don't converge with the real life conditions in which these devices are used. For joint operation of feeling, limbing and buckling shares of the total operating time of the device for idling, working under full load and racing are

approximately equal to 10/55/35% [5]. As a consequence, the chainsaw catalog data regarding the intensity of the harmful agents should be treated orientationally. Taking into account the mentioned shares of the total operating time of the device, the equation (1) takes the following form:

$$a_{\text{hv,eq,R}} = \sqrt{\frac{1}{10} a_{\text{hv,ID}}^2 + \frac{11}{20} a_{\text{hv,FL}}^2 + \frac{7}{20} a_{\text{hv,RA}}^2} \quad (2)$$

where: $a_{\text{hv,eq,R}}$ – real equivalent vibration level.

There are a number of factors that influence the level of vibrations emitted by the chainsaws [6-13]. These factors can be broadly divided into three groups:

- the workpiece (grade, size, physical condition, cellular structure, transverse and longitudinal cuts),
- personal traits of the operator (physique, experience, working position),
- the device and the tool (construction and equipment, power, guide length, chain pitch, engine suspension, cutting chain design).

Neither the influence of the type of cutting tooth design (full chisel and semi-chisel chains), nor chain's wear influence on the vibrations of handles was mentioned in the literature. Because of the adverse health effects of vibration information on this matter is important [14, 15].

2. Measurements

The purpose of the study was to determine the relations between both the wear and the design of the cutting tooth and the level of vibration of the chainsaw. Authors stated a hypothesis that there is a linear, increasing relation between wear and vibration accelerations for each tooth design. In addition, it was assumed that the full chisel chain is favourable (lower acceleration values) for the operator.

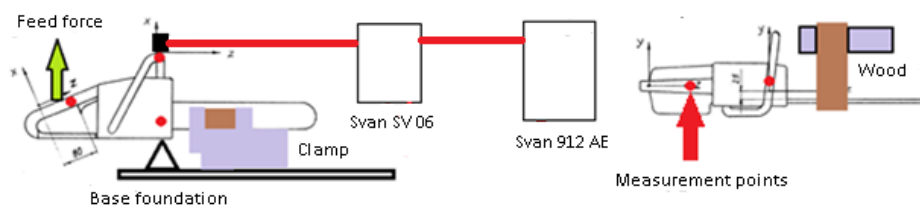


Figure 1. The scheme of the stand and the measurement track

As a part of the study, for both the handles, 9 measurement series were performed. The total recording time of each series was at least 30-second long. Pine beams (90×70 mm) in an air-dry condition were cut. Each of the measurement series was carried out after reaching a specified wear measured by the total cut area (TCA) of 0.5 m². As reported by Maciak [10] the efficiency of the cutting process falls by approximately 13% after cutting 3.5 m². TCA before the last series was equal 4 m². Above in the Figure 1 a scheme of the

stand and the measurement track is shown. In the Figure 2 there are photographs of this stand.

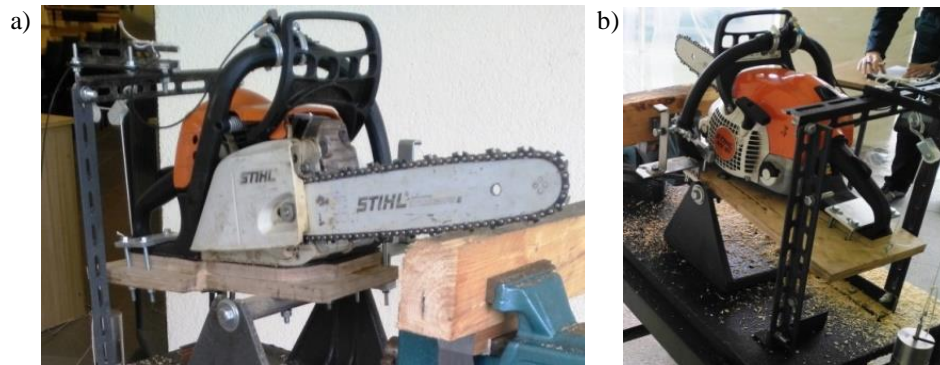


Figure 2. Measurement stand; a) – front view, b) – rear view

The frequency-weighted (correction characteristic W_h) RMS value of the vibration acceleration a_{wh} was the measured parameter. The STIHL MS 181 chainsaw powered by internal combustion engine (1.5 kW) was used during the tests. Measurements were conducted at the stand that:

- compensated the influence of the individual operator's traits,
- provided a constant run of the force (generated by the mass and set of rollers),
- provided fixation of the cut beam (see Figures 1 and 2).

The three-axial vibration transducer DYTRAN 3023M was used to measure vibration accelerations. The analogue vibration signal has been conditioned and processed in the 4-channel data acquisition module SVAN SV 06 cooperating with the vibration meter SVAN 912 AE. Each of the cutting chains was pre-tensed identically before the measurements. Reference axes have been oriented in accordance with ISO 7505: 1986 and ISO 22867: 2011 [1, 2].

3. Research results

The results of measurements of frequency-weighted RMS values of vibration accelerations a_{wh} are presented below. The results are shown firstly for the front handle (left hand) while working with the full chisel chain (Fig. 3) and then while working with the semi-chisel chain (Fig. 4). The results for the rear handle (right hand) while working with the same chains (Fig. 5 and 6) are presented next. Additionally the cumulative means of acceleration values of the chainsaw handles measured under full load, while racing and while idle are shown in the Figures 7 and 8.

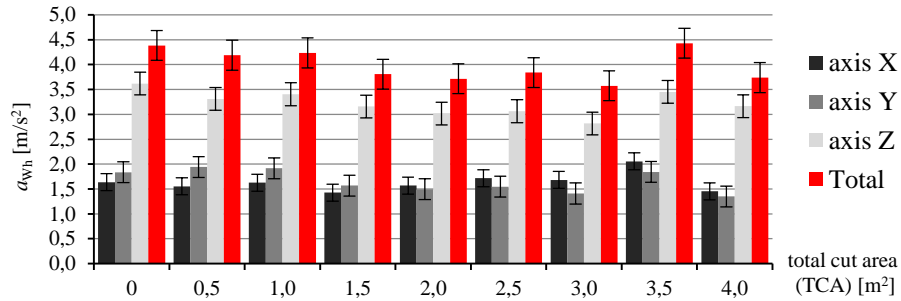


Figure 3. Vibration accelerations of front handle a_{wh} – full chisel chain

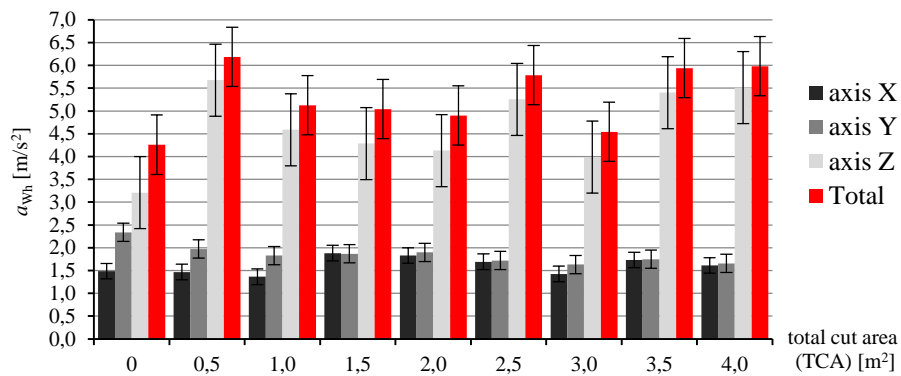


Figure 4. Vibration accelerations of front handle a_{wh} – semi-chisel chain

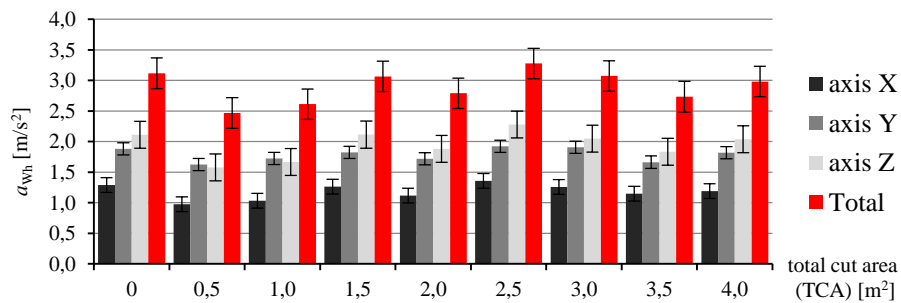


Figure 5. Vibration accelerations of rear handle a_{wh} – full chisel chain

As it can be seen in the Figures 3 and 4, the wear of the cutting teeth, under measuring conditions specified earlier, does not affect the level of vibrations of the front handle. Although the cutting tooth design itself has a significant influence on the vibration levels, that are, on average, 1.3 m/s² higher for the semi-chisel chain. The dominant direction of

the vibrations of the front handle of the chainsaw is the Z direction - the longitudinal axis of the chain guide bar.

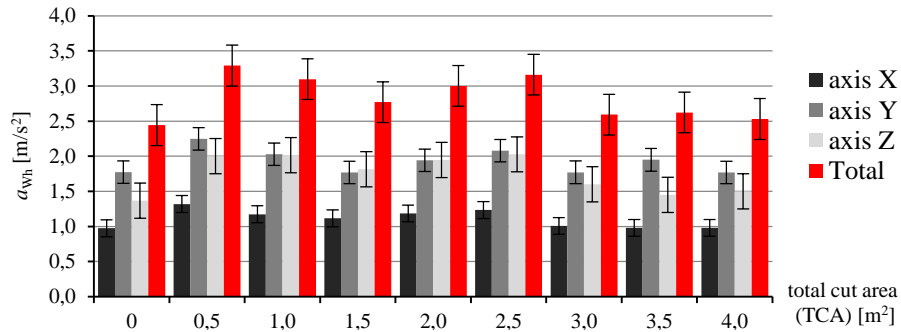


Figure 6. Vibration accelerations of rear handle a_{wh} – semi-chisel chain

As it can be seen in the Figures 5 and 6, the wear of the cutting teeth, under measuring conditions specified earlier, also does not influence the level of vibrations of the rear handle. On the other hand, in contrast to the front handle, the cutting tooth design itself does not affect the vibrations recorded on the rear handle. The dominant directions of the vibrations of the rear handle of the chainsaw are the Z and Y directions - the longitudinal axis of the guide bar and the direction perpendicular to its plane.

Basing on an analysis of cumulative average of vibration accelerations, the full chisel chain performs better than semi-chisel chain, both for the front and the rear handles, (see Figures 7 and 8). There was no dependence between the wear of the full chisel chain and the level of vibrations noted.

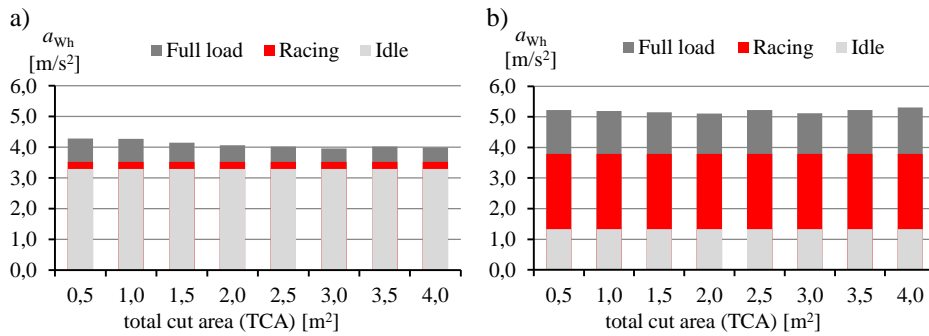


Figure 7. Cumulative averages of vibration accelerations of chainsaw handles for the full chisel chain, a) front handle, b) rear handle

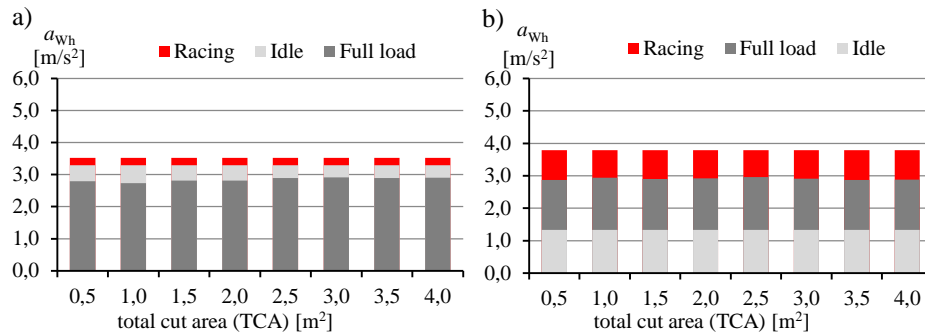


Figure 8. Cumulative averages of vibration accelerations of chainsaw handles for the semi-chisel chain, a) front handle, b) rear handle

The wear of semi-chisel chain has no influence on vibration level of the chainsaw in measuring conditions specified earlier. Comparison of frequency-weighted RMS values of vibration accelerations a_{wh} , measured for three operation modes, allow us to state that the use of equation (1) in order to evaluate the impact of vibrations on a chainsaw operator lowers the real result. Table 1 shows the equivalent vibration level of the tested chainsaw calculated in accordance to standardized conditions [1, 2] (1) and in accordance to real data [5] (2).

Table 1. The equivalent vibration level of the chainsaw STIHL MS 181

shares of the total operation time of the device		$a_{hv,eq}$ [m/s^2]	$a_{hv,eq,R}$ [m/s^2]	$a_{hv,eq,R} - a_{hv,eq}$
		$\frac{1}{3}, \frac{1}{3}, \frac{1}{3}, [1,2]$	$\frac{1}{10}, \frac{11}{20}, \frac{7}{20}, [5]$	$a_{hv,eq,R}$
full chisel chain	front handle	3.61	3.77	4.06%
	rear handle	2.86	3.14	8.79%
semi-chisel chain	front handle	4.14	4.57	9.49%
	rear handle	2.84	3.10	8.51%

The value of $a_{hv,eq}$ calculated according to (1) is on average 7.71% lower than that calculated on the basis of real shares of the total operation time.

Table 2 shows the pictures of the cutting teeth both of designs tested: new and worn (after cutting the total area of 4 m^2).

Table 2. The comparison of cutting teeth, new and used ones

	full chisel chain		semi-chisel chain	
	undamaged	used (TCA = 4 m ²)	undamaged	used (TCA = 4 m ²)
right tooth				
left tooth				

As a result of the visual evaluation of the wear the full chisel chain looks better. In its case, the wear occurs mainly in the form of blunting the nose. On the other hand, the semi-chisel teeth wear on the entire length of the front cutting edge.

4. Conclusions

Basing on the experiment, the results of the measurements and observations, it was found that the full chisel chain provides up to 50% more cutting efficiency under the same conditions than the semi-chisel chain.

The design of a tooth has a significant influence on the level of vibrations of the front handle. The vibration levels measured for the semi-chisel chain was on average 30% higher than the vibration levels measured for the full chisel chain. Higher vibration levels were recorded on the front handle for both of the cutting tooth designs used. The greatest influence on the vibration levels among all variables on the testing stand was the structure of the cut beam (knots, cracks e.g.).

During the measurements, no clear signs of wear of the full chisel chain were noticed. In case of semi-chisel chain a significant cutting edge damage was observed, which is contrary to the data provided by the manufacturer.

No relation between the wear of the cutting teeth measured by TCA and the vibrations recorded on both handles was noted for both of full chisel and semi-chisel chains. Therefore, the assumptions were not confirmed. The chosen measurement methodology does not provide clear and precise possibilities of determining the influence of the cutting tooth design as well as its wear on the vibration level of the chainsaw handles. It is necessary to apply more advanced methods of the vibration signal analysis e.g. time-frequency analysis.

Acknowledgment

The results presented are results of the research that was funded with grant 02/21/DSMK/3482 for education allocated by the Ministry of Science and Higher Education of the Republic of Poland.

References

1. ISO 7505:1986, *Forestry machinery – Chain saw – Measurement of hand-transmitted vibration*.
2. ISO 22867:2011, *Forestry and gardening machinery – Vibration test code for portable hand-held machines with internal combustion engine – Vibration at the handle*.
3. ISO/NP 22868, *Forestry and gardening machinery – Noise test code for portable hand-held machines with internal combustion engine – Engineering method*.
4. Dyrektywa 2006/42/WE Parlamentu Europejskiego i Rady z dn. 17 V 2006 w sprawie maszyn, zmieniająca dyrektywę 95/16/WE.
5. K. Wójcik, *Analisis of processing operation time and his percent share in timber harvesting with the chainsaw*, Annals of Warsaw University of Life Sciences – SGGW, Agriculture, **50** (2007) 71 – 77.
6. K. Wójcik, *Influence of the size of chainsaw and lenght of the guide bar on vibrations emmited during delimiting*, Nauka Przyroda Technologie, **24** (2012) 1 – 12.
7. J. Skarżyński, K. Wójcik, *Timber hardness impact on the level of vubrations I.C.E.-powered sawing machine grips during cutting*, Inżynieria Rolnicza, **99** (2008) 345 – 351.
8. J. Skarżyński, K. Wójcik, *The impact of work technique during timber cutting on vibration and forces on I.C.E.-powered sawing machine grips*, Inżynieria Rolnicza, **99** (2008) 425 – 431.
9. J. Skarżyński, *Influence of wood diameter on the level of vibrations on chainsaw handles during wood cutting*, Technika Rolnicza Ogrodnicza Leśna, **5** (2007).
10. A. Maciak, *The impact of initial tension on rapidity of dulling of saw cutting chains during cross-cutting of pine wood*, Annals of Warsaw University of Life Sciences – SGGW, Agriculture, **66** (2015) 89 – 98.
11. W. Stempski, K. Jabłoński, J. Wegner, *Effect of the edge geometry in a cutting chain on the saw vibration level*, Acta Scientiarum Polonorum, **9** (2010) 25 – 33.
12. W. Stempski, K. Jabłoński, J. Wegner, *Relations between top-plate filling angle values of cutting chains and chainsaw vibration levels*, Acta Scientiarum Polonorum, **9** (2010) 31 – 39.
13. A. Maciak, A. Gendek, *Effect of cutting with the chainsaw with two pairs of cutting link per section*, Annals of Warsaw University of Life Sciences – SGGW, Agriculture, **50** (2015) 59 – 63.
14. J. Malinowska-Borowska, V. Socholik, B. Harazin, *The Health condition of forest workers exposed to noise and vibration produced by chainsaw*, Medycyna Pracy, **63** (2012) 19 – 29.
15. W. Ł. Nowacka, T. Moskalik, *The negative effects of working in forestry with special focus on timber harwesting*, Forrestry Letters, **105** (2013).